3-2017

Climate change impacts on southern Ross Sea phytoplankton composition, productivity, and export

Daniel E. Kaufman
Virginia Institute of Marine Science

Marjorie A. M. Friedrichs
Virginia Institute of Marine Science

Walker O. Smith Jr.
Virginia Institute of Marine Science

Eileen E. Hofmann

Michael S. Dinniman

See next page for additional authors

Recommended Citation

Kaufman, Daniel E.; Friedrichs, Marjorie A. M.; Smith, Walker O. Jr.; Hofmann, Eileen E.; Dinniman, Michael S.; and Hemmings, John C. P., Climate change impacts on southern Ross Sea phytoplankton composition, productivity, and export (2017). *Journal of Geophysical Research: Oceans*, 122(3), 2339-2359. https://doi.org/10.1002/2016JC012514

AGU PUBLICATIONS

JGR

Journal of Geophysical Research: Oceans

RESEARCH ARTICLE

10.1002/2016JC012514

Climate change impacts on southern Ross Sea phytoplankton composition, productivity, and export

Daniel E. Kaufman[1], Marjorie A. M. Friedrichs[1], Walker O. Smith Jr.[1], Eileen E. Hofmann[2], Michael S. Dinniman[2], and John C. P. Hemmings[3,4]

[1]Virginia Institute of Marine Science, College of William and Mary, Gloucester Point, Virginia, USA, [2]Center for Coastal Physical Oceanography, Old Dominion University, Norfolk, Virginia, USA, [3]Wessex Environmental Associates, Salisbury, UK, [4]Now at Met Office, Exeter, UK

Key Points:
- Climate model scenarios for mid-21st and late-21st century indicate increases of primary productivity and carbon export flux
- Shallower mixed layer depths cause diatoms to increase and Phaeocystis antarctica to decrease by the mid-21st century
- Earlier availability of low light from melting sea ice causes Phaeocystis antarctica to increase more than diatoms in the late-21st century

Supporting Information:
- Supporting Information S1
- Table S1

Correspondence to:
D. Kaufman,
dekaufman@vims.edu

Citation:
Kaufman, D. E., M. A. M. Friedrichs, W. O. Smith Jr., E. E. Hofmann, M. S. Dinniman, and J. C. P. Hemmings (2017), Climate change impacts on southern Ross Sea phytoplankton composition, productivity, and export, *J. Geophys. Res. Oceans*, *122*, 2339–2359, doi:10.1002/2016JC012514.

Received 27 OCT 2016
Accepted 22 FEB 2017
Accepted article online 27 FEB 2017
Published online 23 MAR 2017

Abstract The Ross Sea, a highly productive region of the Southern Ocean, is expected to experience warming during the next century along with reduced summer sea ice concentrations and shallower mixed layers. This study investigates how these climatic changes may alter phytoplankton assemblage composition, primary productivity, and export. Glider measurements are used to force a one-dimensional biogeochemical model, which includes diatoms and both solitary and colonial forms of *Phaeocystis antarctica*. Model performance is evaluated with glider observations, and experiments are conducted using projections of physical drivers for mid-21st and late-21st century. These scenarios reveal a 5% increase in primary productivity by midcentury and 14% by late-century and a proportional increase in carbon export, which remains approximately 18% of primary production. In addition, scenario results indicate diatom biomass increases while *P. antarctica* biomass decreases in the first half of the 21st century. In the second half of the century, diatom biomass remains relatively constant and *P. antarctica* biomass increases. Additional scenarios examining the independent contributions of expected future changes (temperature, mixed layer depth, irradiance, and surface iron inputs from melting ice) demonstrate that earlier availability of low light due to reduction of sea ice early in the growing season is the primary driver of productivity increases over the next century; shallower mixed layer depths additionally contribute to changes of assemblage composition and export. This study further demonstrates how glider data can be effectively used to facilitate model development and simulation, and inform interpretation of biogeochemical observations in the context of climate change.

Plain Language Summary Understanding how the global ocean responds to climate change requires knowing the natural behavior of individual regions and anticipating how future changes will affect each region differently. It is especially important to determine these behaviors for regions changing in unique ways and for regions relatively undisturbed by human influences. One such region is the Ross Sea, which has some of the most productive marine plants and animals around Antarctica. Significant changes in the Ross Sea environment are likely over the next century, but it is not known how these changes will impact the marine food web. In this study, computer simulations give us an idea of how warmer temperatures combined with other changes related to melting sea ice may impact the base of the Ross Sea food web over the next century. The simulations show changes in algae species, increases in the amount of plant matter produced, and increases in the amount of plant matter that sinks from the well-lit ocean surface to deeper waters. The details of what cause these changes in the simulations give us new ways of thinking about change in the Ross Sea and point us toward parts of the system warranting further study.

1. Introduction

The Ross Sea is a highly productive marginal sea in the Pacific sector of the Southern Ocean. The continental shelf contained within this sea is the most productive province of the Southern Ocean, with annual production averaging ~180 g C m^{-2} yr^{-1} [*Arrigo et al.*, 2008]. Estimates of vertical carbon export have varied substantially, ranging from ~1% [*Collier et al.*, 2000] to >50% of annual productivity [*Sweeney et al.*, 2000]. High productivity in the Ross Sea polynya is driven by two functional groups, the haptophyte *Phaeocystis*

antarctica that initially dominates the annual bloom, and diatoms, which accompany *P. antarctica* early in the season and regularly form a subsequent bloom later in the season. *P. antarctica* growth begins in late-October soon after sea ice retreat is initiated and open-water polynyas form, allowing sunlight to penetrate the water column [*Smith and Gordon*, 1997]. Mixed layers are still relatively deep during this early phase of the growing season when *P. antarctica* dominate the assemblage. Within days to weeks, the colonial form of *P. antarctica* becomes a larger constituent than solitary cells [*Smith et al*., 2003a]. As time progresses, these colonies undergo senescence and solitary cells are liberated [*Smith et al*., 2017]. *P. antarctica* are rarely present by late-February or March when sea ice again covers the area. Chlorophyll concentrations, as well as primary productivity, typically peak in December [*Arrigo et al*., 2000; *Smith et al*., 2003b]. Early studies described the pattern of biomass accumulation as unimodal [e.g., *Smith et al*., 2000], but further evidence demonstrated that during the latter part of the season there is often a secondary biomass peak as diatoms increase substantially and in some years dominate the phytoplankton [*Peloquin and Smith*, 2007; *Smith et al*., 2010]. The mechanisms allowing diatoms to bloom after *P. antarctica* decline are not fully understood, as it is typically assumed that micronutrient resources (iron) are depleted late in the growing season and would limit further growth.

Environmental conditions are critical in determining how the composition and dynamics of the phytoplankton vary throughout the growing season. Observations from an autonomous glider in 2010–2011 [*Smith et al*., 2014b] suggested that a transition of the phytoplankton assemblage from *P. antarctica* to diatoms was associated with a change in the ratio of carbon to chlorophyll [*Kaufman et al*., 2014]. Analysis of the oceanographic conditions showed this change to be most highly correlated with temperature; however, it was not clear whether the correlation represented a causal relationship or a coincident seasonal trend. Wind, and its effect on mixing, has been implicated as another important factor in determining phytoplankton dynamics in the Ross Sea [*Long et al*., 2012; *Neale et al*., 2012; *Queste et al*., 2015; *Jones and Smith*, 2017]. Other studies have investigated links between phytoplankton and oceanographic variables. For example, an investigation using structural equation modeling and data from January to February 2012 found summer phytoplankton growth rates in the Ross Sea to be most affected by levels of iron [*Mosby and Smith*, 2016]. Irradiance levels likewise have been found to differentially affect phytoplankton growth in the Ross Sea [*Garcia et al*., 2009; *Mills et al*., 2010; *Feng et al*., 2010].

On decadal time scales, the Ross Sea has been experiencing changes in both its physical and biological conditions. Summer temperatures in the atmosphere have been increasing over several decades at McMurdo station, located on Ross Island on the southwestern continental shelf, and in the surrounding water [*Jacobs and Giulivi*, 2010; *LaRue et al*., 2013], even though winter temperatures in the northwestern margin of the Ross Sea have been decreasing [*Sinclair et al*., 2012]. Along with climatic change in temperatures, sea ice and vertical mixing are changing in the Ross Sea. Average sea ice extent and duration have in general been increasing throughout the Ross Sea since at least the 1990s [*Comiso and Nishio*, 2008; *Cavalieri and Parkinson*, 2008; *Stammerjohn et al*., 2008; *Sinclair et al*., 2014], but within the Ross Sea polynya there have also been slight increases in the number of ice-free days between 1992 and 2013 [*Schine et al*., 2015]. A marked freshening of the Ross Sea has been observed since the midtwentieth century, increasing the buoyancy of surface waters and likely diminishing vertical exchange [*Jacobs et al*., 2002; *Jacobs and Giulivi*, 2010]. Additionally, the timing and magnitude of primary productivity in the Ross Sea have been changing over the past two decades [*Arrigo et al*., 2008; *Montes-Hugo and Yuan*, 2012; *Schine et al*., 2015]. Between 1997 and 2013, trends in annual net primary production have been correlated with the number of ice-free days and have been generally increasing in the area of the Ross Sea polynya, but decreasing to the east and northwest [*Schine et al*., 2015].

Climate model projections suggest the trend of increasing sea ice extent over the past several decades is unlikely to continue into the future, but how this will impact the phytoplankton is unknown. The Ross Sea is expected to experience warming throughout the next century along with reduced summer sea ice concentrations and shallower mixed layers [*Bracegirdle et al*., 2008; *Bracegirdle and Stephenson*, 2012]. *Smith et al*. [2014a] utilized 21st century projections of winds and atmospheric temperature from a global climate model, along with a boundary-imposed freshening [*Jacobs and Giulivi*, 2010], to force regional simulations of physical conditions within the Ross Sea for the mid-21st and late-21st century (described further in section 2.2.2). Their simulations with a coupled sea-ice circulation-ice shelf model suggest a summertime expansion of the Ross Sea polynya and shallower mixed layer depths over the next century. There have been efforts to

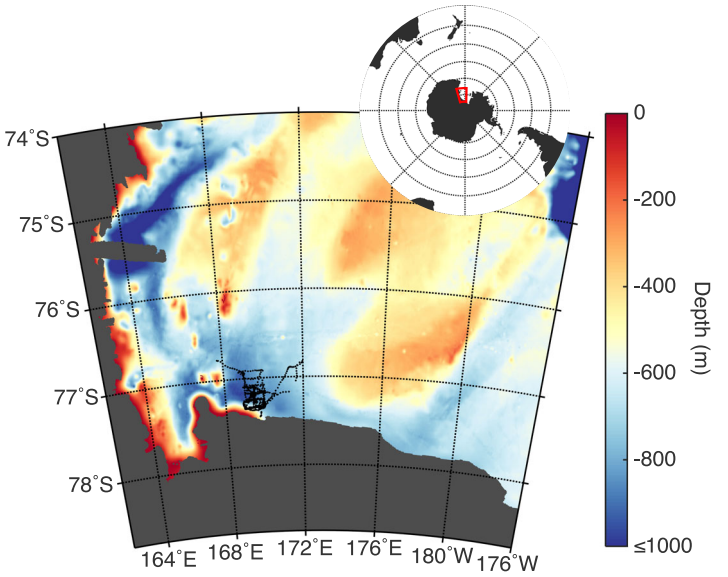

Figure 1. Southwestern Ross Sea showing the glider transect, overlaid on bedmap2 bathymetry of the shelf [*Fretwell et al.*, 2013]. Dark gray areas represent topography above sea level or glacial ice.

interpret the effects that similar physical changes will have on higher trophic levels in the West Antarctic Peninsula [e.g., *Ballerini et al.*, 2014], but the few projections of future biogeochemical conditions in the Ross Sea utilize coarse resolutions and parameter sets not specific to this region, making them unsuitable for detailed region-specific analysis. For instance, a study of Earth System Models in the Coupled Model Intercomparison Project 5 (CMIP5) showed a general trend of increasing surface chlorophyll and integrated primary production by the end of the 21st century over a broad area of the Ross Sea that included both the open ocean and continental shelf [*Rickard and Behrens*, 2016]. However, the authors themselves point out that "the broad range of solutions of the climate scale models for the Ross Sea suggests care has to be taken in translating processes at the relatively large scale of these models to the regional scales." Furthermore, global model projections of phytoplankton do not include dynamics that are specific to this region, such as *P. antarctica* morphotype transitions, thus limiting their effectiveness in evaluating future changes in the Ross Sea. Although some lab studies have attempted to predict how Ross Sea phytoplankton will be altered in the next century [*Xu et al.*, 2014; *Zhu et al.*, 2016], understanding how phytoplankton dynamics are likely to respond to the full range of environmental changes in the Ross Sea remains an open question.

To improve our understanding of ecosystem responses to future physical changes in the southern Ross Sea, we applied a novel one-dimensional (1-D) modeling approach that includes *P. antarctica* morphotype transitions and utilizes high-resolution glider data (Figure 1) for forcing and evaluation. Specifically, simulations were first conducted for a contemporary time period to coincide with the approximate time and location of the glider deployment, allowing for a robust skill assessment of the biogeochemical model. A 1-D test bed framework, designed for comprehensive model analysis, was used to drive the biogeochemistry. This framework allows for direct application of observation-based physical forcing fields derived from the glider data. Subsequently, potential effects of climate-induced changes on Ross Sea biogeochemistry were investigated by running the model under scenarios of future conditions and comparing the results to those of the contemporary setting. The independent contribution of likely changes in different forcing variables was also examined, facilitated by the use of the 1-D analysis framework. In this paper, the structure, forcings, and skill assessment of the model are first described in section 2 before analyzing the results of the contemporary and future scenarios along with their sensitivity to physical and biological inputs in section 3. The implications of these model results are then discussed in section 4 in relation to our understanding of changing biogeochemical dynamics in the Ross Sea, and conclusions are given in section 5.

2. Methods

2.1. Modeling Approach

The biogeochemical Model of Ecosystem Dynamics, nutrient Utilisation, Sequestration and Acidification (MEDUSA) [*Yool et al.*, 2011] was adapted for the Ross Sea and run within the Marine Model Optimization Testbed (MarMOT), an advanced open-source 1-D model analysis framework [*Hemmings and Challenor*, 2012; *Hemmings et al.*, 2015].

2.1.1. MEDUSA Model Structure

MEDUSA is a lower trophic level model with two phytoplankton and zooplankton groups (diatom and non-diatom phytoplankton; microzooplankton and mesozooplankton), two detrital classes, and three nutrients: dissolved silicic acid (DSi), dissolved iron (DFe), and dissolved inorganic nitrogen (DIN). In earlier analyses, data assimilation experiments have been used to demonstrate that models with two phytoplankton and two zooplankton groups represent a good balance of realism and skill for lower trophic level models [*Xiao and Friedrichs*, 2014]. MEDUSA is also well suited for study of the Ross Sea in part because of its inclusion of iron and silicon dynamics. A complete description of MEDUSA-1.0 is given by *Yool et al*. [2011].

MEDUSA has several notable characteristics. Nitrogen is the model's primary "currency," but the model allows phytoplankton to have different C:N ratios and diatoms to have a variable Si:N ratio. Temperature-dependent growth of phytoplankton is limited simultaneously by available light and nutrients. Diatoms incorporate silicic acid and are grazed by mesozooplankton but not microzooplankton. Detritus is remineralized throughout the water column and is modeled in two separate ways: slow-sinking detritus is represented explicitly as a tracer whereas fast-sinking detritus is tracked implicitly as it traverses the water column. Microzooplankton mortality contributes nitrogen and iron directly to the slow-detritus tracer, but not to the fast-sinking flux. Another feature of MEDUSA is that nitrate and ammonium are not included as independent state variables; DIN represents the sum of both. The model includes an iron submodel (adopted from *Parekh et al*. [2005] and based on *Dutkiewicz et al*. [2005]), which distinguishes between "free" iron, which is removed throughout the water column by scavenging, and ligand-bound forms. Rather than explicit modeling of iron complexation reactions, the ratio of "free" and ligand-bound iron scales nonlinearly with total iron concentration according to parameters of total ligand concentration and ligand binding strength. Sinking flux and remineralization in MEDUSA are implemented using a ballast scheme that "protects" a variable fraction of sinking material by inorganic ballasting minerals.

2.1.2. Modifications to MEDUSA

Adaptation of MEDUSA-1.0 for the Ross Sea implementation (MEDUSA-RS) included replacing the original non-diatom tracer with two semi-independent tracers representing *P. antarctica*. Solitary cells of *P. antarctica* (P_s) and colonies of *P. antarctica* (P_c) are divided to represent the morphotype transitions that this species undergoes during growth in the Ross Sea. Concentrations of *P. antarctica* and diatoms are modeled as

$$\frac{\partial P_s}{\partial t} = PP_{P_s} \cdot P_s + C_L - C_F - G_{\mu_{Ps}} - G_{m_{Ps}} - \mu_{1,P_s} \cdot P_s - \mu_{2,P_s} \cdot \frac{P_s}{k_{P_s} + P_s} \cdot P_s, \tag{1}$$

$$\frac{\partial P_c}{\partial t} = PP_{P_c} \cdot P_c + C_F - C_L - \mu_{1,P_c} \cdot P_c - W_{P_c}, \tag{2}$$

$$\frac{\partial P_d}{\partial t} = PP_{P_d} \cdot P_d - G_{m_{Pd}} - \mu_{1,P_d} \cdot P_d - \mu_{2,P_d} \cdot \frac{P_d}{k_{P_d} + P_d} \cdot P_d - W_{P_d}, \tag{3}$$

where PP_{P_x} represents gross primary productivity of phytoplankton type x (and P_x signifies the biomass of a particular group: P_d for diatoms, P_c for *P. antarctica* colonies, and P_s for solitary *P. antarctica*), which is limited by temperature, light, and nutrients; G_μ and G_m represent grazing by microzooplankton and mesozooplankton, respectively; μ_{1,P_x} represents density-independent losses such as respiration; $\mu_{2,P_x} \cdot \frac{P_x}{k_{P_x}+P_x} \cdot P_x$ represents other nonlinear mortalities such as disease or grazing by implicit higher trophic levels; and W_{P_x} represents passive sinking. The two transitions of *P. antarctica*, solitary cells forming colonies (C_F) and solitary cells being liberated from colonies (C_L), are represented in a manner adapted from *Popova et al*. [2007] with the following equations:

$$C_F = \begin{cases} c_F \cdot P_s \cdot (1 - f_z) \cdot Q_{Fe,P_c}, & \text{if } P_s \geq \tau \\ 0, & \text{if } P_s < \tau \end{cases}, \tag{4}$$

$$C_L = c_L \cdot P_c \cdot f_z \cdot \left(1 - Q_{Fe,P_c}\right), \tag{5}$$

where c_F is the max rate of colony formation, c_L is the max rate of solitary cell liberation, Q is a nutrient limitation factor based on Michaelis-Menten kinetics, τ is the threshold concentration at which solitary cells undergo colony formation, f_z is a nondimensional switch that allows colonies to form in the photic zone and solitary

Table 1. Parameter Values Used in This Study

Parameter Name	Symbol	*Phaeocystis antarctica* Colonies, *P. antarctica* Solitary, Diatoms	Units	Reference
C:Chl ratio	C:Chl	40, 30, 150		*DiTullio and Smith* [1996], *Mathot et al.* [2000][a]
C:N molar ratio	C:N	7.3, 7.3, 6.4		*Arrigo et al.* [2000], *Mills et al.* [2010]
Maximum growth rate at 0°C	V	0.5, 0.5, 0.375	d^{-1}	*Smith and Gordon* [1997], *Smith et al.* [1999][a]
Chl-specific initial slope of P-E curve	α	3, 3, 0.6	gC (g chl)$^{-1}$ (W m^{-2})$^{-1}$ d^{-1}	*Mills et al.* [2010][a]
Half saturation conc. for Fe uptake	k_{Fe}	0.1, 0.05, 0.005	mmol N m^{-3}	*Coale et al.* [2003], *Garcia et al.* [2009],[a] *Sedwick et al.* [2007]
Half saturation conc. for DIN uptake	k_N	0.5, 0.5[b], 0.75[b]	mmol N m^{-3}	*Yool et al.* [2011]
Metabolic loss rate	μ_1	0.02, 0.02[b], 0.02[b]	d^{-1}	*Yool et al.* [2011]
Mortality half saturation conc.	k_{mort}	0, 0.5[b], 0.25	mmol N m^{-3}	*Yool et al.* [2011][a]
Maximum gravitational sinking rate	W_{max}	20, 0[b], 5	m d^{-1}	*Smith et al.* [2011][a]
P. antarctica maximum colony formation rate	c_F	5	d^{-1}	*Popova et al.* [2007][a]
P. antarctica threshold solitary cell conc. for colony formation	τ	0.4	mmol N m^{-3}	*Popova et al.* [2007][a]
P. antarctica maximum rate of solitary cell liberation from colonies	c_L	1.6	d^{-1}	*Popova et al.* [2007][a]
		Microzooplankton, Mesozooplankton		
Maximum grazing rate	g	0.3, 0.225	d^{-1}	*Yool et al.* [2011][a]
Grazing half saturation concentration	k_{graz}	0.2, 0.1	mmol N m^{-3}	*Yool et al.* [2011][a]

[a]Value has been modified from the reference value as a result of sensitivity tests.
[b]Value is unchanged from *Yool et al.* [2011].

cells to be liberated when colonies are below the photic zone ($f_z = 0.5 \cdot \left(\tanh\left(\frac{z - z_{ph}}{10}\right) + 1\right)$), and z_{ph} is the photic zone depth. These transitions are calculated slightly differently than *Popova et al.* [2007], to include DFe limiting the formation and maintenance of *P. antarctica* colonies ($Q_{Fe,Pc}$ term in equations above: see supporting information Table S2 for more details); the parameters for the transition equations (c_F, c_L, τ) have also been modified slightly from the values in *Popova et al.* [2007] based on results of sensitivity tests.

Further changes to the model include the addition of sinking terms in the *P. antarctica* colonies and diatom equations. These terms approach a maximum sinking rate (W_{P_x}) as the phytoplankton become increasingly nutrient limited:

$$W_{P_c} = W_{P_{cmax}}\left(1 - \min\left(Q_{N,P_c}, Q_{Fe,P_c}\right)\right), \tag{6}$$

$$W_{P_d} = W_{P_{dmax}}\left(1 - \min\left(Q_{N,P_d}, Q_{Fe,P_d}, Q_{Si}\right)\right). \tag{7}$$

Export flux of carbon at a particular depth in the model is thus calculated as the combination of passively sinking live *P. antarctica* colonies and diatoms with slow sinking of small detrital particles and ballasted fast sinking of large detritus. The aggregation of sinking particles is not modeled explicitly.

Several key parameters were also changed from MEDUSA-1.0 to be more representative of conditions for the Ross Sea (Table 1). For example, distinct C:Chl ratios [*Ditullio and Smith*, 1996] and C:N ratios [*Arrigo et al.*, 2000] were set for each phytoplankton group. In contrast to the setup described by *Yool et al.* [2011], MEDUSA-RS also does not include aeolian deposition. A sensitivity analysis revealed that realistic concentrations of atmospheric iron deposition in the Ross Sea negligibly affect the modeled phytoplankton, in accordance with field-based estimates [*Winton et al.*, 2014]. All model equations are provided in the supporting information Tables S1 and S2.

2.1.3. Physical 1-D Model Framework

MEDUSA-RS was run within the Marine Model Optimization Testbed (MarMOT), which allowed for standardized specification of input files and rapid execution of multiple model runs. MarMOT does not solve for physical variables prognostically. Instead, temperature and vertical diffusivity are provided as inputs (section 2.2). In this study, diffusive motion is assumed to drive all vertical transport and therefore vertical advection is set to zero. The model is configured to focus on dynamics within the euphotic zone, with a domain spanning the ocean surface to 200 m and a vertical resolution of 5 m.

2.2. Model Forcings

Model simulations were conducted at 169°E, 77.4°S in the southern Ross Sea (Figure 1) for the time period 1 October 2012 to 1 February 2013 to coincide with the approximate time and location of an autonomous

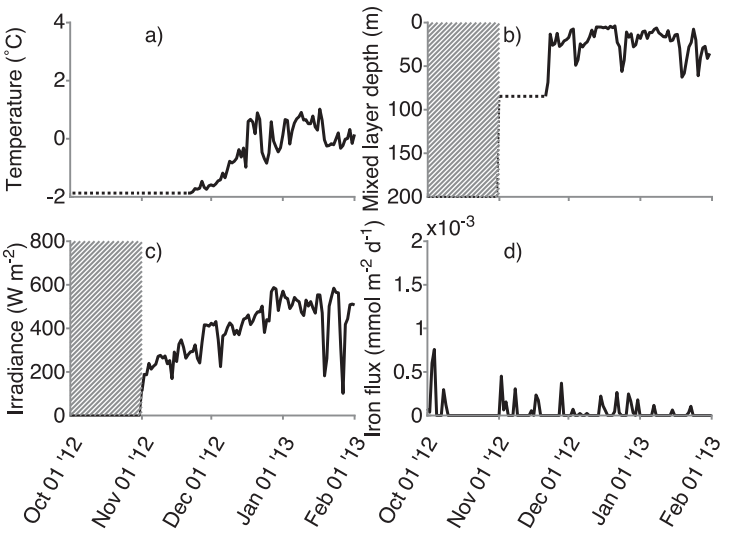

Figure 2. Physical forcings used for the model control run. (a) Sea surface temperature, (b) mixed layer depth, (c) maximum daily irradiance, and (d) surface iron flux. Dotted lines before 22 November 2012 indicate times prior to the first measurements of the glider; hatched areas indicate times before the IMD.

iRobot Seaglider deployment [*Ainley et al*., 2015; *Jones and Smith*, 2017]. This facilitated using the glider data to derive physical forcings for model integration over this time period, which we term the contemporary control run (or simulation; section 2.2.1). The remaining physical forcings for the control run are derived from satellite and reanalysis data. Climate scenario forcings were generated from a regional Ross Sea hydrodynamic model (section 2.2.2), and boundary conditions were set using climatological conditions (section 2.2.3).

2.2.1. Physical Forcings for Contemporary Control Run

Glider data (Figure 1) [*Ainley et al*., 2015; *Jones and Smith*, 2017], available in the BCO-DMO data repository (http://www.bco-dmo.org/dataset/568868), were used to generate the temperature and vertical diffusivity time series required to implement the 1-D model. When available, temperatures were used to force the model directly; prior to the glider deployment (22 November) temperatures in the model were set to the first temperature profile measured by the glider (Figure 2a). After ice no longer covered the ocean surface, mixed layer depths (MLD) were calculated from glider density profiles using a threshold criterion of 0.01 kg m^{-3} [*Kaufman et al*., 2014; *Jones and Smith*, 2017], and were set to the first glider-determined MLD before the glider deployment (Figure 2b; during ice covered time periods the water column was assumed to be well mixed) [*Gordon et al*., 2000]. Following the approach of *Llort* [2015], vertical diffusivities, κ_z, were generated by separating the water column into an upper actively mixed layer and a bottom layer of low mixing. Diffusivity at the surface ($\kappa_z = 10^{-3.5}$ m^2 s^{-1}) was reduced slightly to account for friction at the air-sea interface, and the gradient between the value within the mixed layer ($\kappa_z = 10^{-0.5}$ m^2 s^{-1}) and below ($\kappa_z = 10^{-3}$ m^2 s^{-1}) was smoothed.

Surface irradiances and surface iron fluxes are also required inputs for the 1-D model. Percent ice cover was obtained from the Special Sensor Microwave Imager/Sounder [*Spreen et al*., 2008] and averaged within a rectangular area (167°E–173°E, 77.5°S–76.6°S) surrounding the glider track. An Ice Melt Day (IMD) was defined as a reference to mark the transition from winter conditions. The IMD was calculated as the first day when ice coverage dropped below a threshold level of 80% and remained below this level for at least 75% of the next 30 days. 1 November was calculated as the IMD for the control run in 2012 (Table 2). Experiments demonstrated that the IMD was not highly sensitive to changes in IMD thresholds. Surface solar radiation, including the effect of cloud cover, was obtained from the 3 h forecast fields of the ERA Interim dataset [*Dee et al*., 2011] at the location 169°E, 77.35°S. These values were multiplied by percent ice cover to generate irradiance values that enter at the water surface (Figure 2c). Although this simplification does not account for the thickness of the ice or other internal properties of the ice, it captures the first-order processes of irradiance attenuation due to the presence of sea ice. Solar radiation values were assumed to be zero before the IMD.

Table 2. Physical Forcings for the Control Run and 2050 and 2100 Climate Scenario Simulations

	Control Run (Average)	2050 (Average)	2100 (Average)
Temperature (SST in °C)	−0.96	−0.67	−0.16
MLD (m)	77	72	55
Irradiance (W m^{-2})	240	254	272
Iron input (day when 50% of initial surface iron has entered the water)	15 Nov	10 Nov	4 Nov
IMD (day)	1 Nov	27 Oct	21 Oct

Input of iron into the water column was assumed to occur when sea ice

melts. To represent this, the simulation time period was initialized with a sea ice inventory of 5.8 μmol Fe m^{-2} [*McGillicuddy et al*., 2015]; decreases in sea ice, which are assumed to represent melting, were used to generate a time series of iron input into the surface model layer (Figure 2d). Although sea ice reduction in the real system is a combination of in-place melting and advection out of the area, the scarcity of data on these processes constrains the simulation to represent melting only. This approach represents a spatial averaging of iron input, and is likely a high estimate. The relative magnitude of iron input was proportional to the magnitude of decrease in sea ice cover from a full 100% whenever sea ice dropped below the previously lowest level of cover. For instance, 10% of the initial inventory would be input into the surface model layer on a day in which sea ice cover decreased a further 10% below the previously lowest ice cover percentage (e.g., from 50% to 40%).

2.2.2. Physical Forcings for Future Climate Scenarios

Forcings for the future climate scenarios were generated using output from simulations of a sea ice-ocean-ice shelf model of the Ross Sea based on the Regional Ocean Modeling System (ROMS) [*Dinniman et al*., 2007, 2011]. This implementation, configured with 5 km horizontal grid spacing, 24 vertical layers, and including a dynamic sea ice model, was used to estimate changes in the physical dynamics of the Ross Sea shelf between a contemporary simulation and midcentury (2046–2050) and late-century (2096–2100) simulations. These future scenarios applied projected wind forcing and atmospheric temperature changes from the CMIP3 A1B emissions scenario of the Max-Planck-Institute European Centre/Hamburg 5 (ECHAM5) global climate model [*Jungclaus et al*., 2006]. The observed freshening of the Ross Sea [*Jacobs et al*., 2002], which is thought to be remotely forced due to an increased advection of low-salinity water from the Amundsen Sea [*Jacobs and Giulivi*, 2010; *Nakayama et al*., 2014], was simulated in the future climate scenarios by simply imposing a freshening at the lateral boundaries. Further details of the ROMS model simulations and projected physical conditions are given by *Smith et al*. [2014a].

Four forcing fields of MEDUSA-RS were altered for the climate scenario experiments: temperature, vertical diffusivity, surface iron input, and solar radiation flux (Table 2). These forcing fields were generated using the ROMS model output fields of sea ice cover, MLD, and temperature. For each of these outputs, difference fields were calculated between the 5 day averages in the last 2 years of either the mid-21st or late-21st century simulations and the last 2 years of the contemporary simulation, following the approach of *Smith et al*. [2014a]. The difference fields of temperature and MLD were spatially averaged within 166°E–174°E and 77.5°S–76°S and interpolated from 5 day averages to daily values over the control simulation time-period to produce projected deviations from the control representative of the study area. These differences were added to the current-day time series to generate the mid-21st and late-21st century fields. The timing of polynya expansion in the ROMS simulations occurs on average 5 and 11 days earlier over the continental shelf in the mid-21st and late-21st century [*Smith et al*., 2014a]; following this trend, the IMD, sea ice cover and surface iron input time series were shifted 5 and 11 days earlier. Future vertical diffusivity fields were generated from the modified IMDs and MLDs, and future irradiances were generated from the modified IMD and sea ice time series. The future irradiances represented here come solely from the projected changes in sea ice, therefore the future scenarios include, in effect, the same cloud cover as the control scenario. Because of the significant uncertainty regarding future changes in the physical forcings, simulations were also conducted in which forcings for the future scenarios were each halved or doubled (section 2.4).

2.2.3. Biogeochemical Initial and Boundary Conditions

Initial and bottom (200 m) boundary conditions for DIN and DSi were generated using monthly climatological data with observations spanning 1970–2003 for the months November through February [*Smith et al*., 2003b]. Average DIN and DSi concentrations were calculated from this climatology within a bounding box of 164°E–176°E and 75°S–78°S, which encompasses the entire 2012–2013 glider track (several other boundaries for this box were tried, but the average concentrations did not depend strongly on the size of the box). Initial profiles of DIN and DSi were set to the climatological values for November, which was the climatological profile earliest in the season and closest to the simulation start date. Bottom boundary values for DIN and DSi remained at the initial condition values until the middle of November, transitioned over 1 month to the climatological 200 m average (30.6 mmol N m^{-3} and 80.2 mmol Si m^{-3}), and then were held constant for the remainder of the simulation time period.

Since climatological DFe data are not available, boundary and initial conditions for dissolved iron were drawn from *Sedwick et al*. [2011], *Marsay et al*. [2014], and *Gerringa et al*. [2015]. Based on data within a bounding box of 166°E–174°E and 77.5°S–76°S, the bottom boundary condition for DFe was set to a

constant 0.2 n*M*, which is also a value attributed to Modified Circumpolar Deep Water (MCDW) [*Gerringa et al*., 2015] and is close to the winter DFe "reserve value" present in the water column after deep convective mixing during winter [*McGillicuddy et al*., 2015]. The DFe initial condition was also set to 0.2 n*M*. Initial nitrogen concentrations of diatoms and solitary *P. antarctica* were each set to 0.05 mmol N m^{-3} (approximately equal to 0.1 μg L^{-1} of chlorophyll), while concentrations of colonial *P. antarctica* were set lower (0.001 mmol N m^{-3}) to allow colony formation to mimic patterns observed in situ. Initial concentrations of both microzooplankton and mesozooplankton were set to 0.005 mmol N m^{-3}, and detritus was set to 0.01 mmol N m^{-3}. Initial and bottom boundary conditions for all biogeochemical variables were the same for the future climate scenarios as in the contemporary run.

2.3. Skill Assessment

Bio-optical measurements from the glider as well as climatological data were used to evaluate the modeled biogeochemical distributions. Fluorescence and optical backscatter counts were measured by the glider using a Wet Labs ECO Puck sensor and converted to concentrations of chlorophyll and particulate organic carbon (POC), respectively, using the regression equations of *Jones and Smith* [2017]. These were binned into daily, 5 m vertical bins and compared to modeled chlorophyll as well as POC, which was computed as the sum of phytoplankton, zooplankton and detrital carbon. Climatological monthly means of chlorophyll, nitrate, and silicic acid from November, December, and January [*Smith et al*., 2003b] were also compared with modeled values of chlorophyll, DIN, and DSi. Dissolved iron values from the literature [*Sedwick et al*., 2011; *Marsay et al*., 2014; *Gerringa et al*., 2015] averaged over the upper 50 m were used for assessing performance of the model.

Model-data fit of the contemporary control run was assessed quantitatively using statistical skill metrics that accentuate specific aspects of model performance [*Stow et al*., 2009; *Olsen et al*., 2016], including root mean squared difference (RMSD), unbiased RMSD, bias, standard deviation, and linear correlation. Bias, unbiased RMSD, and RMSD were plotted using Target diagrams [*Hofmann et al*., 2008; *Jolliff et al*., 2009; *Friedrichs et al*., 2009]. Target diagrams provide a straightforward method to compare multiple simulations in terms of bias (*y* axis), unbiased RMSD (*x* axis), and total RMSD (distance from origin). Target diagrams also provide information on whether the modeled standard deviation is greater than that of the observations (model symbols fall to the right of the *y* axis) or less than that of the observations (model symbols fall to the left of the *y* axis). To determine the robustness of model skill assessment results to uncertainty in the parameters and boundary conditions, the contemporary simulation was run with modified (±20%, consistent with variability of DIN and DSI in the climatology) values of nutrient boundary conditions (bottom conditions and initial conditions) and parameters that directly affect phytoplankton growth, *P. antarctica* morphotype transition, and sinking. These sensitivity runs were ranked according to normalized percent differences in RMSD (summed for both chlorophyll and POC) between each sensitivity run and the control run, and model skill was assessed via Target diagrams for simulations in which the five parameters to which chlorophyll and POC were most sensitive were modified.

2.4. Future Scenarios

To examine how Ross Sea phytoplankton composition, productivity and export may change in the future, MEDUSA-RS was run with projected climate forcings (section 2.2.2) and results were compared with the contemporary control run (section 2.2.1). Two scenarios were evaluated, forced by projected conditions for a midcentury period and a late-21st century period (as described in section 2.2.2), and these are hereafter referred to as the 2050 and 2100 future scenarios, respectively. Changes from the contemporary control to a future scenario are denoted by Δ (e.g., ΔPP_{2050} for change in primary productivity from the control to 2050 or ΔE_{2100} for change in export from the control to 2100). Unless otherwise indicated, integrated primary productivity and export values are integrated both over the model depth (200 m) and the simulation time period (1 October 2012 to 1 February 2013) and given in units of g C m^{-2} yr^{-1}. (Note, although these values do not represent integrations over the entire year, roughly 90% of total production occurs before February (W. Smith, personal communication, 2016).

In addition to examining the overall effect of projected changes in the four combined physical forcings, the effect of each forcing change was examined independently while keeping the other three forcings the same as in the contemporary control run. Although in reality, physical drivers of the ecosystem are not independent from each other, these independent tests help to determine the robustness of the future scenario

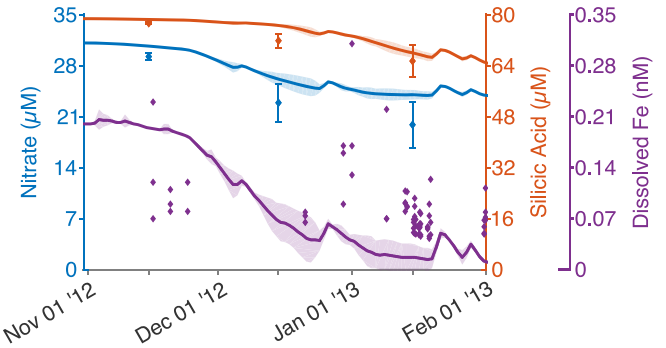

Figure 3. Mean daily modeled DIN (blue line), DSi (orange line), and DFe (purple line) for the upper 50 m of the control run; shaded areas show standard deviations. Dots for nitrate and silica represent climatological values with error bars of one standard deviation for the upper 50 m. Dots for iron represent upper 50 m values from the literature.

results to uncertainty in the representation of the projected environmental changes and to assess the linearity of the simulated effects from changing physical forcings. For this purpose, simulations were also conducted in which forcings for the future scenarios were each halved or doubled. Furthermore, robustness of the future scenario results to uncertainty in parameters and boundary conditions was determined from runs with modified (±20%) values of nutrient boundary conditions (bottom conditions and initial conditions) and parameters that directly affect phytoplankton growth, *P. antarctica* morphotype transition, and sinking. For the sake of focusing on the effect of projected environmental changes, values of ΔPP and ΔE for these sensitivity runs were calculated with respect to the contemporary simulations with similarly modified parameters and boundary conditions.

3. Results

3.1. Contemporary Control Run

3.1.1. Assessment of Chlorophyll and POC

The model results reproduce the drawdown of nutrients observed in climatological data over the growing season (Figure 3), and the pattern of this progression follows changes in the physical drivers. For example, small peaks in nutrient concentrations occur in the model at the same time as short-term mixing events (e.g., on 5 December and 26 December; Figures 2b and 3). By mid-December, most of the sea ice has disappeared and temperatures are as high as 1°C (Figure 2). By this time, when mixed layers are shallow and light levels are approaching their maxima, concentrations of DIN within the upper 50 m have been reduced from their initial condition to an average of ~26 mmol N m^{-3}, a decrease similar to the climatological trend (Figure 3). DSi is drawn down only slightly by 15 December, and less than in the climatological data; however, by 15 January modeled DSi concentrations match the climatology closely (Figure 3). Over this time period, DFe is reduced by more than either DIN or DSi, reaching approximately one third of its initial concentrations by 15 December, matching the range of observed values. Although there are additional inputs of iron in the model at the surface from melting sea ice (Figure 2d), these do not drastically change the dissolved iron concentrations averaged over the top 50 m, which reach low levels near the end of the simulation (Figure 3).

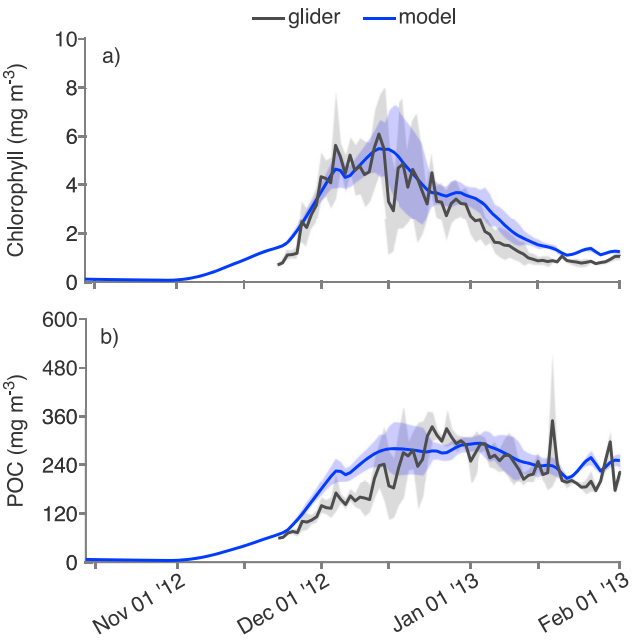

Figure 4. Mean daily modeled biomass from the control run (blue line) and the glider (black line) over the upper 50m for (a) chlorophyll and (b) total POC, with shaded areas representing one standard deviation.

Modeled distributions of chlorophyll and POC compare well with available data (Table 3). In both the control simulation and glider observations,

Table 3. Statistical Comparison Between Biomass Values of Control Run and Glider Observations Averaged Over the Upper 50 m

	Bias	RMSD	Correlation	Model Mean ± Standard Deviation	Glider Mean ± Standard Deviation
Chlorophyll (mg m^{-3})	0.41	0.7	0.94	3.0 ± 1.4	2.6 ± 1.6
POC (mg m^{-3})	27	45	0.84	237 ± 55	210 ± 69

chlorophyll peaks in December and decreases thereafter (Figure 4a). The maximum in chlorophyll occurs after irradiance exceeds ~400 W m^{-2} (Figure 2c), but irradiance continues to increase throughout the second half of December, while chlorophyll concentrations begin to decrease. Average concentrations of modeled chlorophyll in the upper 50 m are highly correlated with measured chlorophyll (Table 3; Figure 4a). Concentrations of POC reach their highest levels in the beginning of January after chlorophyll peaks, and remain elevated throughout the model simulation (Figure 4b). Upper 50 m averages of modeled POC are strongly correlated with glider observations (Table 3; Figure 4b).

Model-data comparison is also visualized using Target diagrams [*Hofmann et al.*, 2008; *Jolliff et al.*, 2009; *Friedrichs et al.*, 2009], for the control run as well as for simulations generated by increasing or decreasing the five parameter or boundary conditions to which modeled chlorophyll and POC were most sensitive (Figure 5). The control run has greater skill, i.e., a lower RMSD, than the mean of the observations, indicating a model efficiency greater than zero [*Stow et al.*, 2009]. For some modified parameter or boundary conditions, total RMSD decreases for either chlorophyll or POC while increasing for the other. For example, increasing the maximum growth rate for diatoms results in a 12% reduction in chlorophyll RMSD but a 22% increase in POC RMSD. Model skill is most sensitive overall to initial and boundary conditions of DFe, for which a 20% decrease or increase results in a 10% reduction or 220% increase of absolute bias in modeled chlorophyll and the greatest departure of total RMSD from the control run. Model skill was also sensitive, albeit less so, to parameters involving *P. antarctica* colonies.

Throughout the simulation, phytoplankton is the largest component of total POC, with zooplankton and detrital biomass making up smaller contributions (Figure 6). Beginning in the latter half of December, and after *P. antarctica* biomass has started to decline, zooplankton carbon increases slowly until the end of the simulation, but remains a small percentage (<10%) of total carbon throughout. These low abundances of zooplankton are in qualitative agreement with cruise measurements showing low heterotrophic plankton abundance in the spring and early summer of 1996–1997 [*Dennett et al.*, 2001]. Detrital carbon is highest at the beginning of January after *P. antarctica* concentrations have started to decline (Figure 6).

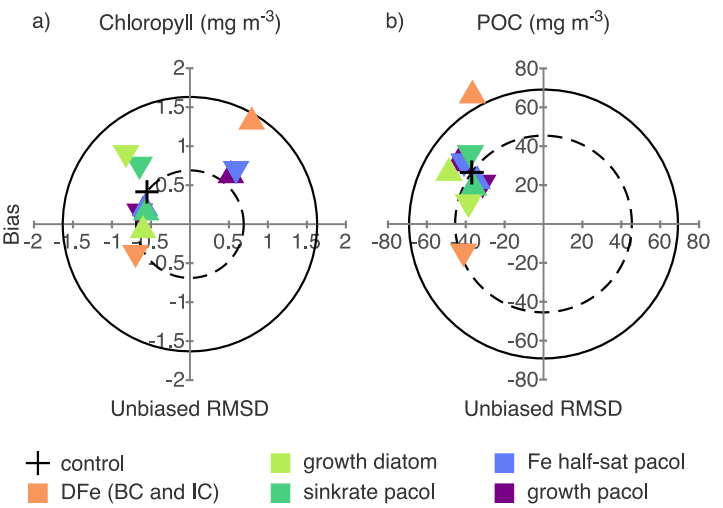

Figure 5. Target diagrams for the control run comparing (a) modeled daily chlorophyll with glider-derived chlorophyll and (b) modeled daily POC with glider-derived POC for the upper 50 m. Skill values are also shown for the top five parameters to which chlorophyll and POC were most sensitive. Upward (downward) pointing triangles indicate runs in which the parameter was increased (decreased) by 20%. The radius of the dashed circle represents the total RMSD of the control run, and the radius of the solid circle represents standard deviation of the glider observations. Abbreviations BC and IC refer to (bottom) boundary condition and initial condition, respectively, and pacol indicates *P. antarctica* colonies.

3.1.2. Assessment of Phytoplankton Assemblage Composition, Productivity, and Export

The relative dominance of *P. antarctica* and diatoms varies throughout the contemporary control simulation (Figures 7a and 7b). Modeled solitary cells of *P. antarctica* begin accumulating around 1 November, slightly earlier than colonies or diatoms, as a result of increased available light, shoaling of the

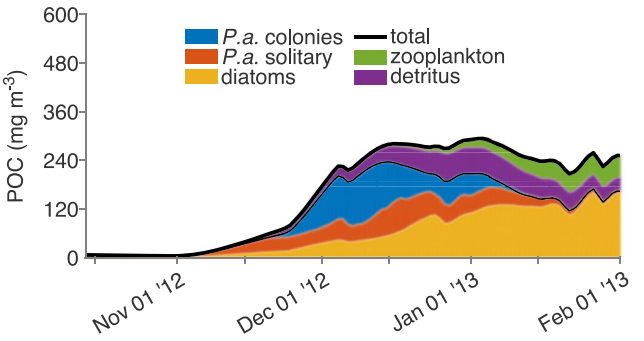

Figure 6. Partitioning of modeled POC into constituent model state variables.

mixed layer and plentiful iron. Soon after their initial growth, solitary *P. antarctica* cells exceed the threshold concentration in the model and begin forming colonies. Colonies then undergo a sharp increase in abundance, becoming maximal in the first half of December (Figures 7a and 7b) when the mixed layer has shoaled to an average of ~20 m (Figure 2b). By the first week of December, average dissolved iron concentrations in the upper 50 m have been reduced from ~0.2 to ~0.14 n*M* due to *P. antarctica* growth (Figure 3). Diatoms accumulate slower than *P. antarctica*, and diatoms are not a major constituent of the assemblage until after mid-December, by which time they average ~50 mg C m^{-3} in the upper 50 m, accounting for >30% of total phytoplankton carbon (Figure 7b), although <10% of total chlorophyll (Figure 7a). *P. antarctica* biomass declines during the latter half of December as irradiance and temperatures continue to increase and mixed layers remain shallow. Diatoms continue growing in January, even while average DFe in the upper 50 m remains less than 0.07 n*M* (Figure 3).

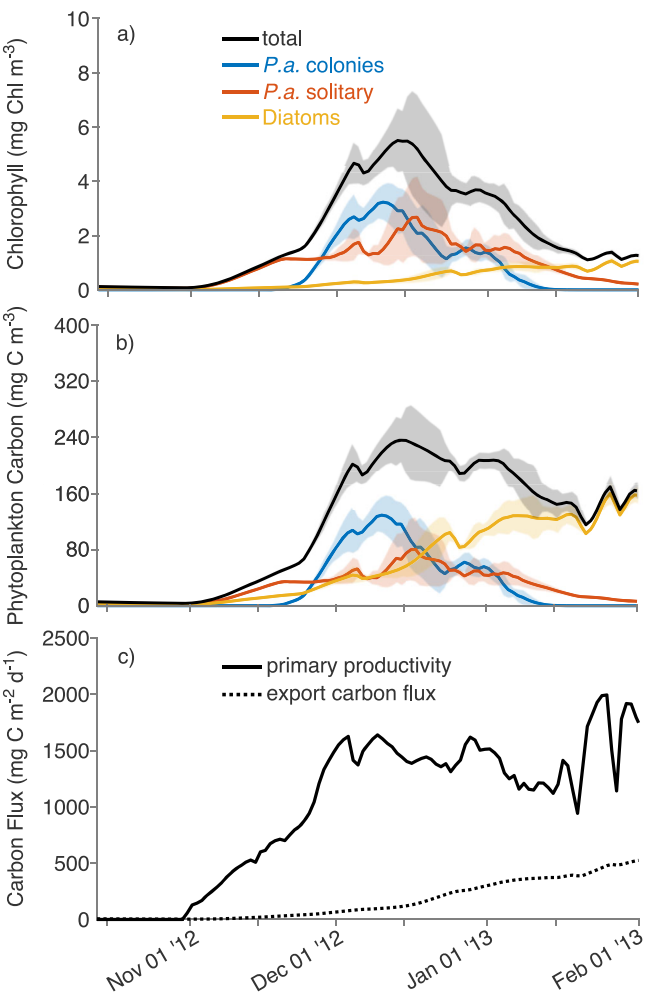

Figure 7. Time series of modeled (a) chlorophyll and (b) carbon for each phytoplankton group averaged over the upper 50 m. Shaded areas represent one standard deviation. (c) Time series of depth-integrated primary productivity (solid line) and carbon export flux at 200 m (dotted line).

Although there are no temporally resolved data sets of in situ assemblage composition to quantitatively compare to for this time/location as was possible for chlorophyll and POC (Figure 5), the temporal shift in partitioning among phytoplankton groups can be compared to other information in the literature. Studies have shown that relative dominance of *P. antarctica* in the assemblage of the Ross Sea polynya tends to reach maxima in December or early January, and colonies are the largest component of *P. antarctica* cells at that time [*Arrigo et al.*, 2000; *Smith et al.*, 2003a,2010,2013]. The model time series generates a peak of *P. antarctica* colonies at a time in agreement with the literature estimates of peak *P. antarctica* abundance (Figure 7). Measurements of cell abundances along cruise transects in the Ross Sea polynya in 1996–1997 found that diatom and flagellated (solitary) *P. antarctica* cell abundances reached maximum abundance between mid-January to late-January [*Smith et al.*, 2003a]. Diatom biomass in the model is consistent with this documented pattern, although modeled solitary *P. antarctica* cells peak just after mid-December (Figures 7a and 7b), which is slightly earlier than measurements by *Smith et al.* [2003a] suggest. Additional pigment and nutrient analyses revealed that

subsequent to spring maxima of *P. antarctica* colonies, diatoms can become either equally dominant with *P. antarctica* or more dominant in late spring and summer [*Smith et al.*, 2006; *Peloquin and Smith*, 2007; *Smith et al.*, 2013], and this is reproduced in the model (Figures 7a and 7b). Glider observations of chlorophyll and POC during 2011 also suggested that a temporal succession from *P. antarctica* to diatoms occurred after 10 January [*Kaufman et al.*, 2014], similar to the pattern followed by phytoplankton chlorophyll (Figure 7a).

The timing of modeled primary production generally follows the pattern of total phytoplankton carbon in the model, with primary productivity integrated over the model simulation reaching 112 g C m^{-2} yr^{-1}. Modeled productivity generally agrees well with Ross Sea estimates computed for other years [*Saba et al.*, 2011] and is not substantially different from estimated annual production of 87 g C m^{-2} yr^{-1} for 2012–2013 computed from MODIS satellite observations for the western Ross Sea [*McGillicuddy et al.*, 2015]. Export flux of organic carbon at 200 m in the model (19 g C m^{-2} yr^{-1}) represents ~17% of total primary production in the overlying water column, but varies from ~2% in early November to a maximum of 42% in late-January (Figure 7c). The mean daily carbon export flux (151 mg C m^{-2} d^{-1}) is within the range of flux estimates reported from elemental budgets, yet higher than estimates of carbon flux from moored sediment traps [*Smith et al.*, 2011b]. Carbon export flux increases more slowly than productivity; a similar lag between productivity and export was observed in 1991–1992, when productivity estimates were maximum in early January while flux estimates were maximum in late-February representing a lag of ~50 days [*Smith and Dunbar*, 1998]. Lags of 4 weeks between productivity and export flux maxima were observed in 2005–2006 as well [*Smith et al.*, 2011b]. Thorium isotope estimates of POC flux at 100 m in this area also indicated a maximum after mid-January 1997 [*Cochran et al.*, 2000]. Carbon export flux begins to increase in the second half of December and throughout January, after the *P. antarctica* have mostly disappeared from the upper waters, reaching ~30–50% of primary productivity in late-January.

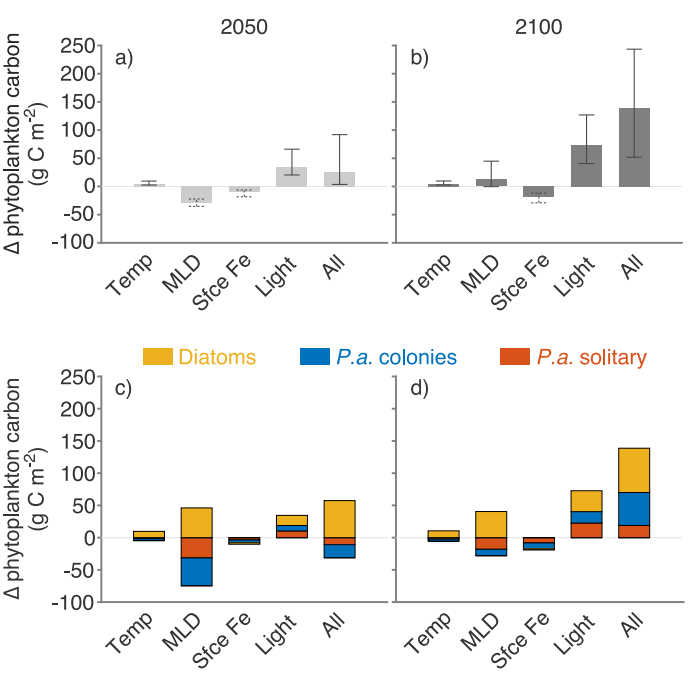

Figure 8. Change in time-integrated (and depth-integrated to 200 m) phytoplankton carbon between the contemporary control run and the (a) mid-21st and (b) late-21st century climate scenarios. Changes in biomass of each phytoplankton group are also shown between the contemporary control run and the (c) mid-21st and (d) late-21st century climate scenarios. Bars indicate changes due to temperature, MLD, surface iron flux, irradiance, and all four forcings combined. The effect of halving and doubling physical forcing deltas (between contemporary and future scenarios) are shown by the capped error bars; the dotted error bars for Fe indicate when doubling (halving) of the delta resulted in a greater (less) reduction in phytoplankton carbon.

3.2. Future Climate Scenarios

3.2.1. Phytoplankton Biomass and Assemblage Composition

Application of mid-21st and late-21st century forcing to MEDUSA-RS yields increases in overall phytoplankton biomass in both future scenarios; however, these increases are dependent on the assumed future physical forcing conditions. Despite significant uncertainties in the future physical forcing (uncertainties in Figures 8a and 8b represent results of doubling and halving future changes in physical forcing), the increase (from the contemporary control run) in phytoplankton biomass is considerably greater in the late-century scenario than in the midcentury scenario (Figures 8a and 8b). Not surprisingly, the uncertainty in phytoplankton biomass in the late-century simulation is much greater than in the midcentury simulation, though both scenarios show increases in biomass.

The simulated changes in biomass result from the unique effects of the four independent physical

forcings (i.e., temperature, MLD, solar radiation flux, and surface iron flux). In particular, earlier influx of solar radiation is the primary driver of increased integrated phytoplankton carbon from the control run to both the midcentury and late-century scenario (Figures 8a and 8b). Changes in MLD, in contrast, result in decreased integrated phytoplankton carbon in the midcentury scenario, which, when combined with the effects of the other physical forcings, results in a smaller increase in biomass for the run with combined forcings. Shifts toward earlier input of iron from melting sea ice have less of an impact than irradiance and MLD midcentury, though earlier input of iron has a moderate negative impact on productivity in the late-century scenario. Temperature increases have positive yet minimal direct impacts on total phytoplankton biomass for both midcentury and late-century.

The three phytoplankton groups respond quite differently to the forcing changes (Figures 8c and 8d). Diatom carbon increases ~60 g C m^{-2} from the control run to midcentury, whereas total *P. antarctica* carbon decreases ~30 g C m^{-2}, with solitary *P. antarctica* biomass decreasing by approximately half as much as colonial *P. antarctica*. These overall changes are largely due to the shallower MLDs of the midcentury forcing (Figure 8c). In the late-century scenario, both diatom and *P. antarctica* biomass are ~70 g C m^{-2} higher than in the contemporary control run, implying a small increase of only ~10 g C m^{-2} in the second half of the 21st century for diatoms and a larger increase of ~100 g C m^{-2} for *P. antarctica*. Again, the impact of temperature on growth and remineralization rates and changes in surface iron flux do not have major impacts on simulated future phytoplankton assemblage composition in the Ross Sea (Figure 8d).

3.2.2. Productivity and Export

Primary productivity and carbon export are greater in both the midcentury and late-century scenarios compared to the control (Figure 9). In addition, productivity and export in the late-century scenario are greater than in the midcentury scenario, although differences between the future scenarios and control are more robust to uncertainties in the future physical forcings than differences between the two future scenarios (uncertainties in Figure 9 represent results of doubling and halving future changes in physical forcing). Integrated productivity increases 6 g C m^{-2} yr^{-1} (5% increase), which is twice as much as carbon export at 200 m increases (3 g C m^{-2} yr^{-1}) from the control run to midcentury (Figures 9a and 9c). Primary productivity is 15 g C m^{-2} yr^{-1} greater (14% increase) in the late-century scenario than the contemporary control run and export flux of carbon increases 4 g C m^{-2} yr^{-1} (Figures 9b and 9d). Throughout the 21st century, carbon export represents ~18% of total primary production. The timing of maximum productivity for the groups change in the future scenarios, with diatoms reaching a productivity maximum in both midcentury and late-century approximately 1 week earlier than in the control; *P. antarctica*, on the other hand, reach maximum productivity 4 and 10 days earlier in the midcentury and late-century scenarios, respectively.

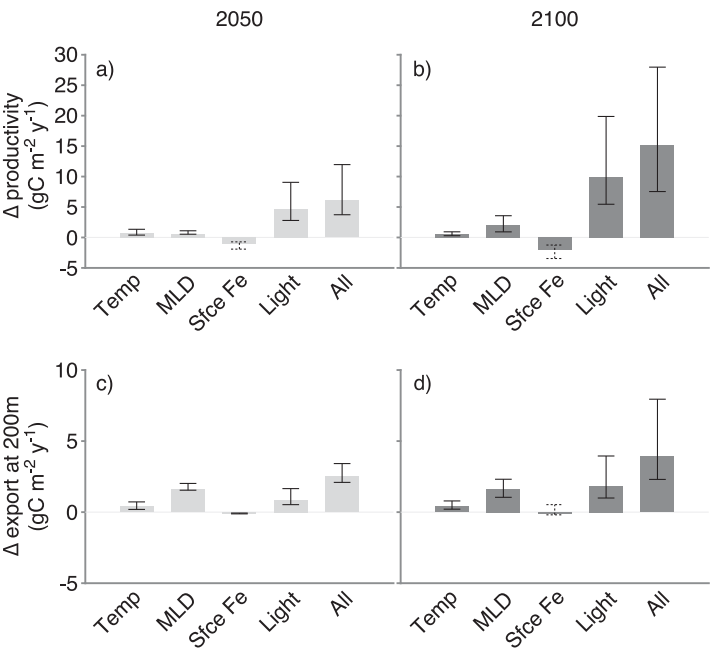

Figure 9. Change in productivity from the contemporary control to the (a) mid-21st and (b) late-21st century climate scenarios, and change in carbon export flux at 200 m from the contemporary control to the (c) mid-21st and (d) late-21st century climate scenarios. The effect of halving and doubling physical forcing deltas (between contemporary and future scenarios) is shown by the capped error bars; the dotted error bars for Fe indicate when doubling (halving) of the delta resulted in a greater (less) reduction in productivity.

Productivity and carbon export flux at 200 m in the future scenarios are affected more by changes in MLD and irradiance than by the direct effect of temperature or changes in surface iron flux from melting ice. Changes in MLD have minor

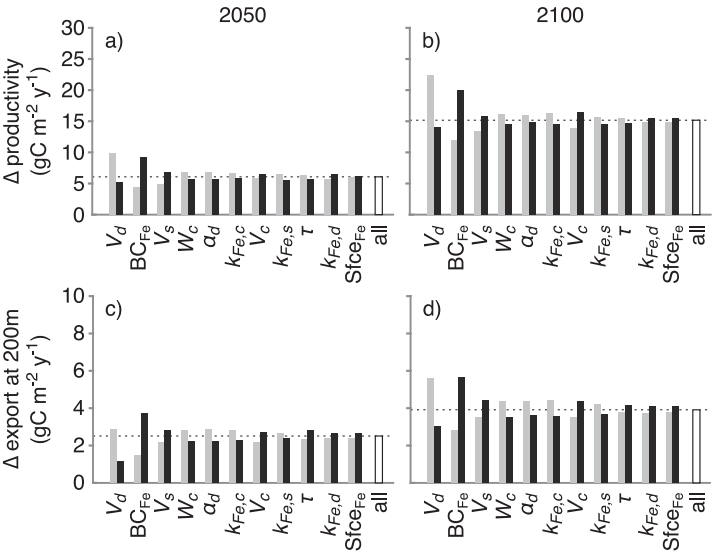

Figure 10. Effects of modified parameter values and boundary conditions on (a, b) productivity and (c, d) export for the future scenarios. The height of each bar represents change from the contemporary control to the future scenarios. Light gray bars on the left of each pair (dark gray bars on the right of each pair) indicate runs in which the parameter or boundary value was decreased (increased) by 20%. Only shown are parameter or boundary conditions for which a 20% change resulted in more than a 5% change in ΔPP or ΔExport. Abbreviations BC_{Fe} and $Sfce_{Fe}$ refer to boundary concentration (including both bottom and initial condition) and surface iron concentration, respectively, and other abbreviations and symbols are identified in Table 1.

impacts on total productivity and are much less than the effects of changes in irradiance (Figures 9a and 9b). In contrast, the magnitude of ΔExport from MLD changes is similar to that from changes in irradiance (Figures 9c and 9d). Shifts in the timing of surface iron input result in lower productivity and carbon export, but these changes are barely significant. The impact of higher temperatures on phytoplankton productivity is generally less than any of the other independent effects, however, runs with higher temperature show a minor increase in carbon export flux for both future scenarios. For both the mid-21st and late-21st century scenarios, the combined effect of the four physical forcing changes on productivity and export is different from a linear summation of their individual effects.

3.2.3. Sensitivity of Scenario Results to MEDUSA-RS Parameters and Boundary Conditions

Simulated changes in productivity and export between the contemporary control run and the future scenarios also depend on boundary conditions and model parameter values (Figure 10). Their impact on projected environmental changes was evaluated by comparing future and contemporary scenarios with similarly modified (±20%) values. Variation in the DFe bottom boundary condition and the maximum growth rate of diatoms results in the greatest change in ΔPP and ΔE estimates. A 20% increase (decrease) in the bottom boundary concentration of DFe results in a 52% increase (27% decrease) in ΔPP in 2050 and a 32% increase (21% decrease) in 2100 (Figure 10). On the contrary, a 20% increase (decrease) in the diatom growth rate results in a 14% decrease (61% increase) in ΔPP in 2050 and a 7% decrease (47% increase) in 2100. Changes in productivity and export were less sensitive to other parameters, such as the phytoplankton sinking rates and half saturation coefficients for iron uptake. The threshold concentration (τ) for *P. antarctica* colony formation affects ΔPP and ΔExport more than the other two morphotypes transition parameters c_F and c_L (Figure 10). The future scenario results were relatively insensitive (<5% change in ΔPP and ΔE) to other parameters, such as the initial slope of the photosynthesis-irradiance curve (α) for solitary *P. antarctica* cells and the boundary values of DIN and DSi.

4. Discussion

4.1. Implications of Future Ross Sea Changes

The simulated future phytoplankton assemblage and productivity changes (Figures 8 and 9) are similar to those hypothesized in the literature. *Smith et al.* [2014a] suggest that production will likely increase due to changes in summer sea ice concentrations and hypothesize that shallower MLDs will cause diatoms to dominate the future phytoplankton assemblage relative to *P. antarctica*. A competition experiment by *Xu et al.* [2014] also suggests that future conditions of light, CO_2, and temperature may favor diatoms over *P. antarctica*. In the lab, results from a culture experiment investigating the interactive effects of temperature and iron led *Zhu et al.* [2016] to conclude that the distribution of diatoms would likely expand relative to *P. antarctica* in the future, primarily due to temperature impacts on growth rate. The simulations here are in accord with these suggestions of increased diatom production for 2050; however, the simulations in this

study suggest that this increased diatom productivity may not continue throughout the second half of the 21st century. Instead, during this later time period, the model projects that increases in *P. antarctica* will exceed those of diatoms as a result of interplay between MLD changes and an earlier beginning of the growing season when ice melts. Additionally, the simulations here suggest direct effects of increased temperature on growth and remineralization rates over the next century will be small compared to effects of changes in MLD and irradiance.

Carbon export is of particular interest in the Ross Sea due to high productivity, and because aggregates appear in a greater abundance than in many other areas of the world [*Asper and Smith*, 2003]. The midcentury model scenario produced both an increase in the relative proportion of diatom productivity and a ~13% increase in export, which contrasts with the hypothesis advanced by *Xu et al*. [2014] that carbon export may decrease as assemblage composition shifts in the future toward more diatoms. Between the midcentury and late-century scenarios, however, the proportion of productivity exported remained nearly constant rather than declining as *P. antarctica* production increased relative to diatoms. Evidence on the relative contribution of diatoms and *P. antarctica* to Ross Sea export is mixed, with some suggestion that diatoms may contribute to carbon export to a lesser extent than *P. antarctica* [*DiTullio et al*., 2000]; however, although diatoms may sink more slowly they also may form more aggregates [*Asper and Smith*, 2003]. In accordance with these observations, *P. antarctica* colonies in the model do sink faster than diatoms, although liberation of solitary cells and remineralization in the model limited export of *P. antarctica*. Recent observations found collapsed *P. antarctica* colonies, known as ghost colonies, below intact colonies; this indicates the possibility of *P. antarctica* contributing greater to carbon flux than hitherto estimated, although the sparseness of observed ghost colonies during the single season of measurements led the authors to concede the possibility of revealing greater contributions of ghost colonies to export flux with more measurements [*Smith et al*., 2017].

Future changes in phytoplankton composition, productivity and export have implications for the rest of the Ross Sea food web. Although it is tempting to speculate that an increase in diatom productivity would provide increased energy to grazers and thus increase secondary production, the Ross Sea is considered a "wasp-waist" food web, in which abundances of middle trophic level taxa are relatively low, despite high primary production and high abundances of higher trophic levels [*Ainley et al*., 2015]. In particular, microzooplankton abundance is demonstrably low in the Ross Sea [*Caron et al*., 2000; *Dennett et al*., 2001], and if zooplankton increases linearly with phytoplankton then low abundances may simply continue over the next century in part because surplus production may be recycled or exported depending on the relative fraction ingested versus egested. The model used here excludes grazing of *P. antarctica* colonies, based on previous studies suggesting *P. antarctica* colonies are ineffectively grazed by zooplankton [*Tang et al*., 2008]. However, other model results suggest that in the Ross Sea polynya low zooplankton abundances may be a result of temporal decoupling from early and rapid growth as opposed to any inherent resistance of *P. antarctica* to zooplankton grazing [*Tagliabue and Arrigo*, 2003].

The MEDUSA-RS model does not explicitly model trophic levels above mesozooplankton, but future contributions to higher trophic level production will likely depend on how relative abundances of diatoms and *P. antarctica* change, regardless of the decoupling versus grazing-resistance mechanism. For example, *Euphausia crystallorophias* is the dominant krill species in the southern Ross Sea [*Sala et al*., 2002], but much is unknown about this species' relationship to phytoplankton. Mesozooplankton abundances on the continental shelf appear to be less than in the open ocean to the North [*Stevens et al*., 2015]. Any interpretation of potential implications for top predators, such as penguins, are tenuous as contemporary observations indicate that primary production in the Ross Sea sometimes, but not always, exhibits covarying relationships with higher trophic level species such as seals and penguins [*Dugger et al*., 2014; *Paterson et al*., 2015; *Ainley et al*., 2015]. For instance, in contrast to East Antarctica where variation in primary production explains 64% of the variation in penguin colony size, in West Antarctica, where the Ross Sea is located, variation in primary production only explains 13% of variation in penguin colony size [*Arrigo and Van Dijken*, 2003].

4.2. Mechanisms of Future Ross Sea Changes

The magnitude and direction of productivity changes in future scenarios simulated here are determined not by one individual environmental driver, but by the interactive effects of multiple factors. Direct effects of temperature on growth and remineralization rates had the smallest impact on primary productivity of

the four manipulated forcings in these model experiments, even when the predicted temperature change was doubled (Figure 9a). Synoptically, satellite observations from 1997 to 2013 reveal a significant positive relationship between temperatures and net primary production [*Schine et al*., 2015], and intraseasonal glider observations show strong correlations between sea surface temperature (SST) and biomass variations in the Ross Sea [*Kaufman et al*., 2014]. However, observed correlations with temperature inherently include indirect effects on other physical conditions such as sea ice, light availability, and surface iron fluxes. Other studies have also shown that temperature changes often have less of an effect alone than when accompanied by concurrent changes in irradiance or nutrients, especially iron. For instance, shipboard incubation experiments found the effects of increased temperature to be generally less than the effects of increased iron concentrations [*Rose et al*., 2009]. Furthermore, structural equation modeling, which is a multivariate statistical analysis technique for determining direct and indirect causal relationships, in the Ross Sea revealed a weaker relationship between phytoplankton and temperature as compared to MLD or iron concentrations [*Mosby and Smith*, 2016]. Manipulation experiments with Ross Sea phytoplankton demonstrated a response by diatoms to increased temperatures, whereas *P. antarctica* did not respond to temperature increases except when accompanied by increased iron as well [*Zhu et al*., 2016]. The simulations here reproduce this differential response, with diatom productivity increasing more than *P. antarctica* in response to increased temperatures.

Vertical mixing, which is strongly regulated by sea ice and wind, is another important factor shaping the phytoplankton assemblage, productivity and export in the Ross Sea. In these simulations, MLD estimates are obtained from glider observations, which implicitly include effects of sea ice and wind. Wind plays an important role in perturbing phytoplankton biomass distributions on intraseasonal timescales throughout the Southern Ocean [*Fitch and Moore*, 2007]. During this particular glider deployment, short-term wind events are implicated in disrupting phytoplankton growth and increasing export flux, especially near the time of peak bloom [*Jones and Smith*, 2017]. Short-term wind events can be considered represented by the changing MLDs observed by the glider. More broadly, the observed freshening of the Ross Sea continental shelf is not solely a result of local atmospheric changes, but rather broader changes such as increased melt water from the Amundsen Sea ice shelves [*Jacobs and Giulivi*, 2010; *Nakayama et al*., 2014]. If this freshening continues, it will lead to MLD shoaling [*Smith et al*., 2014a] that drives the changes in phytoplankton composition simulated here.

This study found primary productivity to be most impacted by changes in irradiance, which is the primary limiting resource in the early period of the growing season and is predominantly regulated by sea ice [*Massom and Stammerjohn*, 2010]. These results suggest that irradiance is not only the primary contemporary factor in regulating phytoplankton production, but future changes in irradiance due to earlier reduction of sea ice can lead to greater changes in phytoplankton production and export than future changes in MLD, timing of surface iron input and temperature. Diatoms and *P. antarctica* have been referred to as "layer formers" and "mixers," respectively, reflecting their different strategies for optimizing carbon fixation under varying light levels [*Cullen and MacIntyre*, 1998; *Kropuenske et al*., 2009]. In future scenarios modeled here, earlier melting of sea ice opens the ocean surface to irradiance during a time when solar radiation levels are lower than later in the season. This extension of the lower light period permits an extended period of growth for *P. antarctica*, which are noted for their relative dominance in conditions of lower light availability [*Arrigo et al*., 1999, 2000, 2010]. In midcentury scenarios this irradiance effect is outweighed by the effect of changes in MLD that enable greater diatom growth just at the time when *P. antarctica* reach maximum biomass in the contemporary system. However, in the late-21st century scenarios the enabling of *P. antarctica* growth under lower surface irradiances offsets the changes in MLD.

4.3. Uncertainties in Future Ross Sea Changes

The use of a one-dimensional (1-D) modeling framework is an experimental design choice, often appropriate because of the importance of vertical exchanges that are critical to plankton dynamics. This approach is frequently a valuable first step before exploring a system with a more computationally intensive 3-D model. The principal advantage of using a 1-D framework is the ability to run a multitude of scenarios relatively quickly for sensitivity experiments or data assimilation experiments aimed at parameter identification [*Schartau et al*., 2016]. A wide array of assimilation experiments permits more in-depth intermodel structural comparisons [*Friedrichs et al*., 2007] and the ability to run large ensemble simulations makes it easier to

explore the effects of uncertainties from various sources [*Hemmings and Challenor*, 2012]. The 1-D setup established here will facilitate a more comprehensive study of uncertainty in future work.

A particular source of uncertainty is the extent to which the observations used, both to drive and evaluate the model, are representative of the wider study area. Model simulations in this study, for example, are not representative of the entire Ross Sea continental shelf, and thus do not include the spatial heterogeneity that is observed in this region [e.g., *Arrigo and McClain*, 1994; *Nelson et al*., 1996; *Sweeney et al*., 2000]. Instead, the 1-D simulations can be considered as representing spatially averaged conditions of the southern Ross Sea. Horizontal advection is assumed to be negligible, even though horizontal transport and eddies may be important near island land masses and the Ross Ice Shelf [*Gerringa et al*., 2015; *Li et al*., 2017]. In principle, uncertainties associated with lateral fluxes could similarly be investigated by using the 1-D test bed framework in conjunction with 3-D model experiments [*Hemmings et al*., 2015]. In addition to spatial considerations, having suitable glider observations from a single year limits the representativeness of the contemporary control simulation. Compared to other years, *Jones and Smith* [2017] report that the 2012–2013 year was warmer, more stratified, and experienced lower average wind speeds. However, ice coverage values and solar radiation time series around the location of the glider indicate that the 2012–2013 year was similar to the 2 years prior and the year after.

It is useful to consider additional sources of uncertainties from model structure, boundary conditions, and parameters. Structural choices during the development of the MEDUSA-RS model determined certain aspects of the scenario results. For example, the method by which the carbon to chlorophyll ratio varied throughout the simulation (fixed for each group, but varying in total with compositional changes) could affect the scenario results. Modeling the morphotype transitions between solitary cells and colonies of *P. antarctica* was achieved in a relatively simple manner but can have a large effect on the consequent simulation results. Here the rates of transition were determined in part by iron limitation, but additional control variables could be included. Although not necessarily a large component of the *P. antarctica* export, ghost colonies may be prevalent within the Ross Sea, and their effect on phytoplankton dynamics should be explored further [*Smith et al*., 2017]. There are also considerable uncertainties in the future physical forcing fields. Here these were estimated by doubling/halving the differences from the current state in the future physical fields. Although these sensitivity experiments demonstrated that the absolute magnitude of productivity and export changes were a direct, though nonlinear, function of the magnitude of future physical changes, the relative magnitudes were not; the relative importance of the four physical forcings, when modified independently, were independent of the absolute magnitude of the future projected change. Finally, there are also uncertainties in parameters and boundary values, which were examined by increasing and decreasing these values by 20%. These modifications were shown to have an impact on the magnitude of modeled future changes in productivity and export although the directions of change were insensitive to these modifications. In general, uncertainties in future irradiances had the largest effects on future productivity and export, although uncertainties in diatom growth rate and boundary concentrations of iron had substantial effects as well. The uncertainties in MLD and timing of surface iron input flux were of similar relative importance as the uncertainties in a few sensitive model parameters, such as the growth rate of *P. antarctica* solitary cells, the sinking rate of *P. antarctica* and the initial P-E slope of diatoms. More robust parameter optimization analyses with MEDUSA-RS are needed to further determine the region of parameter space that is most consistent with the contemporary observations and to estimate future scenario uncertainties by down-weighting results for parameters that are less consistent with contemporary observations. Work toward this goal is currently underway using the data assimilative capabilities of MarMOT [*Hemmings and Challenor*, 2012].

5. Conclusions

The impacts of projected environmental changes on Ross Sea phytoplankton were investigated with the MEDUSA-RS biogeochemical model, and results of these changes in forcing provide three main findings. First, future changes in physical condition lead to increases in total primary productivity and carbon export flux over the 21st century. Second, between the contemporary and midcentury simulations, diatoms increase while *P. antarctica* decrease, whereas in the late-21st century *P. antarctica* increase while diatom biomass changes very little. This is because in midcentury the effects of irradiance changes are outweighed

by MLD changes, whereas in the late-century scenario earlier melting of sea ice extends the growing season of *P. antarctica* earlier into a period of lower average irradiances. Third, the overall increased irradiance from melting sea ice drives primary production increases, however shallower MLDs additionally cause increased export and assemblage changes. There is often difficulty teasing apart mechanistic relationships from in situ measurements alone, and application of biogeochemical models is often limited by the quantity and type of in situ data appropriate for evaluation and forcing. The use of glider measurements, to generate physical forcings and evaluate in situ biomass, along with a 1-D model here demonstrates the effectiveness of a synthetic approach, which partly overcomes the individual limitations of these otherwise distinct approaches.

Acknowledgments

This material is based upon work supported by the U.S. National Science Foundation's Office of Polar Programs (NSF-ANT-0838980). This paper is contribution 3607 of the Virginia Institute of Marine Science, College of William and Mary. This work was performed (in part) using computational facilities at the College of William and Mary which were provided by contributions from the National Science Foundation, the Commonwealth of Virginia Equipment Trust Fund and the Office of Naval Research. The authors would like to thank two anonymous reviewers and Elizabeth Canuel for providing constructive comments in revision of the manuscript. Data from the autonomous glider are available from the BCO-DMO data repository (http://www.bco-dmo.org/dataset/568868), and other data to support this article are available at W&M Publish (http://doi.org/10.21220/V5PC71) and upon request from the authors (dekaufman@vims.edu, marjy@vims.edu).

References

Ainley, D. G., G. Ballard, R. M. Jones, D. Jongsomjit, S. D. Pierce, W. O. Smith Jr., and S. Veloz (2015), Trophic cascades in the western Ross Sea, Antarctica: Revisited, *Mar. Ecol. Prog. Ser.*, *534*, 1–16, doi:10.3354/meps11394.

Arrigo, K. R., and C. R. McClain (1994), Spring phytoplankton production in the western Ross Sea, *Science*, *266*(5183), 261–263, doi:10.1126/science.266.5183.261.

Arrigo, K. R., and G. L. Van Dijken (2003), Phytoplankton dynamics within 37 Antarctic coastal polynya systems, *J. Geophys. Res.*, *108*(C8), 3271, doi:10.1029/2002JC001739.

Arrigo, K. R., D. H. Robinson, D. L. Worthen, R. B. Dunbar, G. R. DiTullio, M. VanWoert, and M. P. Lizotte (1999), Phytoplankton community structure and the drawdown of nutrients and CO_2 in the Southern Ocean, *Science*, *283*, 365–367, doi:10.1126/science.283.5400.365.

Arrigo, K. R., G. R. Ditullio, R. B. Dunbar, D. H. Robinson, M. VanWoert, D. L. Worthen, and M. P. Lizotte (2000), Phytoplankton taxonomic variability in nutrient utilization and primary production in the Ross Sea PP in the Ross, *J. Geophys. Res.*, *105*(C4), 8827–8846, doi:10.1029/1998JC000289.

Arrigo, K. R., G. L. van Dijken, and S. Bushinsky (2008), Primary production in the Southern Ocean, 1997–2006, *J. Geophys. Res.*, *113*, C08004, doi:10.1029/2007JC004551.

Arrigo, K. R., M. M. Mills, L. R. Kropuenske, G. L. van Dijken, A.-C. Alderkamp, and D. H. Robinson (2010), Photophysiology in two major southern ocean phytoplankton taxa: Photosynthesis and growth *of Phaeocystis antarctica* and *Fragilariopsis cylindrus* under different irradiance levels, *Integr. Comp. Biol.*, *50*(6), 950–66, doi:10.1093/icb/icq021.

Asper, V. L., and W. O. Smith Jr. (2003), Abundance, distribution and sinking rates of aggregates in the Ross Sea, Antarctica, *Deep Sea Res., Part I*, *50*(1), 131–150, doi:10.1016/S0967-0637(02)00146-2.

Ballerini, T., E. E. Hofmann, D. G. Ainley, K. Daly, M. Marrari, C. A. Ribic, W. O. Smith Jr., and J. H. Steele (2014), Productivity and linkages of the food web of the southern region of the western Antarctic Peninsula continental shelf, *Prog. Oceanogr.*, *122*, 10–29, doi:10.1016/j.pocean.2013.11.007.

Bracegirdle, T. J., and D. B. Stephenson (2012), Higher precision estimates of regional polar warming by ensemble regression of climate model projections, *Clim. Dyn.*, *39*(12), 2805–2821, doi:10.1007/s00382-012-1330-3.

Bracegirdle, T. J., W. M. Connolley, and J. Turner (2008), Antarctic climate change over the twenty first century, *J. Geophys. Res.*, *113*, D03103, doi:10.1029/2007JD008933.

Caron, D. A., M. R. Dennett, D. J. Lonsdale, D. M. Moran, and L. Shalapyonok (2000), Microzooplankton herbivory in the Ross Sea, Antarctica, *Deep Sea Res., Part II*, *47*, 3249–3272, doi:10.1016/S0967-0645(00)00067-9.

Cavalieri, D. J., and C. L. Parkinson (2008), Antarctic sea ice variability and trends, 1979–2006, *J. Geophys. Res.*, *113*, C07004, doi:10.1029/2007JC004564.

Coale, K. H., X. Wang, S. J. Tanner, and K. S. Johnson (2003), Phytoplankton growth and biological response to iron and zinc addition in the Ross Sea and Antarctic Circumpolar Current along 170 W, *Deep Sea Res., Part II*, *50*, 635–653, doi:10.1016/S0967-0645(02)00588-X.

Cochran, J. K., K. O. Buesseler, M. P. Bacon, H. W. Wang, D. J. Hirschberg, L. Ball, J. Andrews, G. Crossin, and A. Fleer (2000), Short-lived thorium isotopes (^{234}Th, ^{228}Th) as indicators of POC export and particle cycling in the Ross Sea, Southern Ocean, *Deep Sea Res., Part II*, *47*(15–16), 3451–3490, doi:10.1016/S0967-0645(00)00075-8.

Collier, R., J. Dymond, S. Honjo, S. Manganini, R. Francois, and R. Dunbar (2000), The vertical flux of biogenic and lithogenic material in the Ross Sea: Moored sediment trap observations 1996–1998, *Deep Sea Res., Part II*, *47*(15–16), 3491–3520, doi:10.1016/S0967-0645(00)00076-X.

Comiso, J. C., and F. Nishio (2008), Trends in the sea ice cover using enhanced and compatible AMSR-E, SSM/I, and SMMR data, *J. Geophys. Res.*, *113*, C02S07, doi:10.1029/2007JC004257.

Cullen, J. J., and J. G. MacIntyre (1998), Behavior, physiology and the niche of depth-regulating phytoplankton, in *Physiological Ecology of Harmful Algal Blooms*, vol. 41, edited by D. M. Anderson, A. D. Cembella, and G. M. Hallegraeff, pp. 559–580, Springer-Verlag, Berlin, Heidelberg.

Dee, D. P., et al. (2011), The ERA-Interim reanalysis: Configuration and performance of the data assimilation system, *Q. J. R. Meteorol. Soc.*, *137*(656), 553–597, doi:10.1002/qj.828.

Dennett, M. R., S. Mathot, D. A. Caron, W. O. Smith Jr., and D. J. Lonsdale (2001), Abundance and distribution of phototrophic and heterotrophic nano- and microplankton in the southern Ross Sea, *Deep Sea Res., Part II*, *48*, 4019–4037, doi:10.1016/S0967-0645(01)00079-0.

Dinniman, M. S., J. M. Klinck, and W. O. Smith Jr. (2007), Influence of sea ice cover and icebergs on circulation and water mass formation in a numerical circulation model of the Ross Sea, Antarctica, *J. Geophys. Res.*, *112*, C11013, doi:10.1029/2006JC004036.

Dinniman, M. S., J. M. Klinck, and W. O. Smith Jr. (2011), A model study of Circumpolar Deep Water on the West Antarctic Peninsula and Ross Sea continental shelves, *Deep Sea Res., Part II*, *58*(13–16), 1508–1523, doi:10.1016/j.dsr2.2010.11.013.

DiTullio, G. R., and W. O. Smith Jr. (1996), Spatial patterns in phytoplankton biomass and pigment distributions in the Ross Sea, *J. Geophys. Res.*, *101*(C8), 18,467–18,477.

DiTullio, G. R., J. M. Grebmeier, K. R. Arrigo, M. P. Lizotte, D. H. Robinson, A. Leventer, J. P. Barry, M. L. VanWoert, and R. B. Dunbar (2000), Rapid and early export of *Phaeocystis antarctica* blooms in the Ross Sea, Antarctica., *Nature*, *404*(6778), 595–598, doi:10.1038/35007061.

Dugger, K. M., G. Ballard, D. G. Ainley, P. O. Lyver, and C. Schine (2014), Adélie penguins coping with environmental change: Results from a natural experiment at the edge of their breeding range, *Front. Ecol. Evol.*, *2*(October), 1–12, doi:10.3389/fevo.2014.00068.

Dutkiewicz, S., M. J. Follows, and P. Parekh (2005), Interactions of the iron and phosphorus cycles: A three-dimensional model study, *Global Biogeochem. Cycles*, *19*, GB1021, doi:10.1029/2004GB002342.
Feng, Y., et al. (2010), Interactive effects of iron, irradiance and CO_2 on Ross Sea phytoplankton, *Deep Sea Res., Part I*, *57*(3), 368–383, doi:10.1016/j.dsr.2009.10.013.
Fitch, D. T., and J. K. Moore (2007), Wind speed influence on phytoplankton bloom dynamics in the Southern Ocean Marginal Ice Zone, *J. Geophys. Res.*, *112*, C08806, doi:10.1029/2006JC004061.
Fretwell, P., et al. (2013), Bedmap2: Improved ice bed, surface and thickness datasets for Antarctica, *Cryosphere*, *7*(1), 375–393, doi:10.5194/tc-7-375-2013.
Friedrichs, M. A. M., et al. (2007), Assessment of skill and portability in regional marine biogeochemical models: Role of multiple planktonic groups, *J. Geophys. Res.*, *112*, C08001, doi:10.1029/2006JC003852.
Friedrichs, M. A. M., et al. (2009), Assessing the uncertainties of model estimates of primary productivity in the tropical Pacific Ocean, *J. Mar. Syst.*, *76*(1–2), 113–133, doi:10.1016/j.jmarsys.2008.05.010.
Garcia, N. S., P. N. Sedwick, and G. R. DiTullio (2009), Influence of irradiance and iron on the growth of colonial *Phaeocystis antarctica*: Implications for seasonal bloom dynamics in the Ross Sea, Antarctica, *Aquat. Microb. Ecol.*, *57*, 203–220, doi:10.3354/ame01334.
Gerringa, L. J. A., P. Laan, G. L. van Dijken, H. van Haren, H. J. W. De Baar, K. R. Arrigo, and A.-C. Alderkamp (2015), Sources of iron in the Ross Sea Polynya in early summer, *Mar. Chem.*, *177*, 447–459, doi:10.1016/j.marchem.2015.06.002.
Gordon, L. I., L. A. Codispoti, J. C. Jennings, F. J. Millero, J. M. Morrison, and C. Sweeney (2000), Seasonal evolution of hydrographic properties in the Ross Sea, Antarctica, 1996–1997, *Deep Sea Res., Part II*, *47*(15–16), 3095–3117, doi:10.1016/S0967-0645(00)00060-6.
Hemmings, J. C. P., and P. G. Challenor (2012), Addressing the impact of environmental uncertainty in plankton model calibration with a dedicated software system: The Marine Model Optimization Testbed (MarMOT 1.1 alpha), *Geosci. Model Dev.*, *5*(2), 471–498, doi:10.5194/gmd-5-471-2012.
Hemmings, J. C. P., P. G. Challenor, and A. Yool (2015), Mechanistic site-based emulation of a global ocean biogeochemical model (MEDUSA 1.0) for parametric analysis and calibration: An application of the Marine Model Optimization Testbed (MarMOT 1.1), *Geosci. Model Dev.*, *8*(3), 697–731, doi:10.5194/gmd-8-697-2015.
Hofmann, E. E., et al. (2008), Eastern US continental shelf carbon budget: Integrating models, data assimilation, and analysis, *Oceanography*, *21*(1), 86–104, doi:10.5670/oceanog.2008.70.
Jacobs, S. S., and C. F. Giulivi (2010), Large multidecadal salinity trends near the Pacific–Antarctic continental margin, *J. Clim.*, *23*(17), 4508–4524, doi:10.1175/2010JCLI3284.1.
Jacobs, S. S., C. F. Giulivi, and P. A. Mele (2002), Freshening of the Ross Sea during the late 20th century, *Science*, *297*(5580), 386–389, doi:10.1126/science.1069574.
Jolliff, J. K., J. C. Kindle, I. Shulman, B. Penta, M. A. M. Friedrichs, R. Helber, and R. A. Arnone (2009), Summary diagrams for coupled hydrodynamic-ecosystem model skill assessment, *J. Mar. Syst.*, *76*(1–2), 64–82, doi:10.1016/j.jmarsys.2008.05.014.
Jones, R. M., and W. O. Smith Jr. (2017), The influence of short-term events on the hydrographic and biological structure of the southwestern Ross Sea, *J. Mar. Syst.*, *166*, 184–195, doi:10.1016/j.jmarsys.2016.09.006.
Jungclaus, J. H., N. Keenlyside, M. Botzet, H. Haak, J.-J. Luo, M. Latif, J. Marotze, U. Mikolajewicz, and E. Roeckner (2006), Ocean circulation and tropical variability in the coupled model ECHAM5/MPI-OM, *J. Clim. Spec. Sect.*, *19*, 3952–3972, doi:10.1175/JCLI3827.1.
Kaufman, D. E., M. A. M. Friedrichs, W. O. Smith Jr., B. Y. Queste, and K. J. Heywood (2014), Biogeochemical variability in the southern Ross Sea as observed by a glider deployment, *Deep Sea Res., Part I*, *92*, 93–106, doi:10.1016/j.dsr.2014.06.011.
Kropuenske, L. R., M. M. Mills, G. L. van Dijken, S. Bailey, D. H. Robinson, N. A. Welschmeyer, and K. R. Arrigo (2009), Photophysiology in two major Southern Ocean phytoplankton taxa: Photoprotection in *Phaeocystis antarctica* and *Fragilariopsis cylindrus*, *Limnol. Oceanogr.*, *54*(4), 1176–1196, doi:10.4319/lo.2009.54.4.1176.
LaRue, M. A., D. G. Ainley, M. Swanson, K. M. Dugger, P. O. Lyver, K. Barton, and G. Ballard (2013), Climate change winners: Receding ice fields facilitate colony expansion and altered dynamics in an Adélie penguin metapopulation, *PLoS One*, *8*(4), 1–7, doi:10.1371/journal.pone.0060568.
Li, Y., D. J. McGillicuddy Jr., M. S. Dinniman, and J. M. Klinck (2017), Processes influencing formation of low-salinity high-biomass lenses near the edge of the Ross Ice Shelf, *J. Mar. Syst.*, *166*, 108–119, doi:10.1016/j.jmarsys.2016.07.002.
Llort, J. (2015), Bloom phenology, mechanisms and future change in the Southern Ocean, doctoral thesis, Univ. Pierre et Marie Curie, Paris.
Long, M. C., L. N. Thomas, and R. B. Dunbar (2012), Control of phytoplankton bloom inception in the Ross Sea, Antarctica, by Ekman restratification, *Global Biogeochem. Cycles*, *26*, GB1006, doi:10.1029/2010GB003982.
Marsay, C. M., P. N. Sedwick, M. S. Dinniman, P. M. Barrett, S. L. Mack, and D. J. McGillicuddy Jr. (2014), Estimating the benthic efflux of dissolved iron on the Ross Sea continental shelf, *Geophys. Res. Lett.*, *41*, 7576–7583, doi:10.1002/2014GL061684.
Massom, R. A., and S. E. Stammerjohn (2010), Antarctic sea ice change and variability—Physical and ecological implications, *Polar Sci.*, *4*(2), 149–186, doi:10.1016/j.polar.2010.05.001.
Mathot, S., W. O. Smith, C. A. Carlson, D. L. Garrison, M. M. Gowing, and C. L. Vickers (2000), Carbon partitioning within *Phaeocystis antarctica* (Prymnesiophyceae) colonies in the Ross Sea, Antarctica, *J. Phycol.*, *36*, 1049–1056, doi:10.1046/j.1529-8817.2000.99078.x.
McGillicuddy, D. J., Jr., et al. (2015), Iron supply and demand in an Antarctic shelf ecosystem, *Geophys. Res. Lett.*, *42*, 8088–8097, doi:10.1002/2015GL065727.
Mills, M. M., L. R. Kropuenske, G. L. van Dijken, A.-C. Alderkamp, G. M. Berg, D. H. Robinson, N. A. Welschmeyer, and K. R. Arrigo (2010), Photophysiology in two southern ocean phytoplankton taxa: Photosynthesis of *Phaeocystis antarctica* (Prymnesiophyceae) and *Fragilariopsis cylindrus* (Bacillariophyceae) under simulated mixed-layer irradiance, *J. Phycol.*, *46*(6), 1114–1127, doi:10.1111/j.1529-8817.2010.00923.x.
Montes-Hugo, M. A., and X. Yuan (2012), Climate patterns and phytoplankton dynamics in Antarctic latent heat polynyas, *J. Geophys. Res.*, *117*, C05031, doi:10.1029/2010JC006597.
Mosby, A. F., and W. O. Smith Jr. (2016), Structural equation modeling of the influence of environmental factors on summer phytoplankton growth in the Ross Sea, *Polar Biol.*, *40*, 291–299, doi:10.1007/s00300-016-1953-7.
Nakayama, Y., R. Timmermann, M. Schröder, and H. H. Hellmer (2014), On the difficulty of modeling circumpolar deep water intrusions onto the Amundsen Sea continental shelf, *Ocean Modell.*, *84*, 26–34, doi:10.1016/j.ocemod.2014.09.007.
Neale, P. J., C. Sobrino, and A. E. Gargett (2012), Vertical mixing and the effects of solar radiation on photosystem II electron transport by phytoplankton in the Ross Sea Polynya, *Deep Sea Res., Part I*, *63*, 118–132, doi:10.1016/j.dsr.2012.01.011.
Nelson, D. M., D. J. DeMaster, R. B. Dunbar, and W. O. Smith Jr. (1996), Cycling of organic carbon and biogenic silica in the Southern Ocean: Estimates of water-column and sedimentary fluxes on the Ross Sea continental shelf, *J. Geophys. Res.*, *101*(C8), 18,519–18,532, doi:10.1029/96JC01573.

Olsen, E., G. Fay, S. Gaichas, R. Gamble, S. Lucey, and J. S. Link (2016), Ecosystem model skill assessment. Yes we can!, *PLoS One*, *11*(1), 1–24, doi:10.1371/journal.pone.0146467.
Parekh, P., M. J. Follows, and E. A. Boyle (2005), Decoupling of iron and phosphate in the global ocean, *Global Biogeochem. Cycles*, *19*, GB2020, doi:10.1029/2004GB002280.
Paterson, J. T., J. J. Rotella, K. R. Arrigo, and R. A. Garrott (2015), Tight coupling of primary production and marine mammal reproduction in the Southern Ocean, *Proc. R. Soc. B*, *282*(1806), 20143137, doi:10.1098/rspb.2014.3137.
Peloquin, J. A., and W. O. Smith Jr. (2007), Phytoplankton blooms in the Ross Sea, Antarctica: Interannual variability in magnitude, temporal patterns, and composition, *J. Geophys. Res.*, *112*, C08013, doi:10.1029/2006JC003816.
Popova, E. E., R. T. Pollard, M. I. Lucas, H. J. Venables, and T. R. Anderson (2007), Real-time forecasting of ecosystem dynamics during the CROZEX experiment and the roles of light, iron, silicate, and circulation, *Deep Sea Res., Part II*, *54*(18–20), 1966–1988, doi:10.1016/j.dsr2.2007.06.018.
Queste, B. Y., K. J. Heywood, W. O. Smith Jr., D. E. Kaufman, T. D. Jickells, and M. S. Dinniman (2015), Dissolved oxygen dynamics during a phytoplankton bloom in the Ross Sea polynya, *Antarct. Sci.*, *27*(4), 362–372, doi:10.1017/S0954102014000881.
Rickard, G., and E. Behrens (2016), CMIP5 Earth System Models with biogeochemistry: A Ross Sea assessment, *Antarct. Sci.*, *28*(5), 1–20, doi:10.1017/S0954102016000122.
Rose, J. M., et al. (2009), Synergistic effects of iron and temperature on Antarctic phytoplankton and microzooplankton assemblages, *Biogeosciences*, *6*, 3131–3147, doi:10.5194/bg-6-3131-2009.
Saba, V. S., et al. (2011), An evaluation of ocean color model estimates of marine primary productivity in coastal and pelagic regions across the globe, *Biogeosciences*, *8*(2), 489–503, doi:10.5194/bg-8-489-2011.
Sala, A., M. Azzali, and A. Russo (2002), Krill of the Ross Sea: Distribution, abundance and demography of *Euphausia superba* and *Euphausia crystallorophias* during the Italian Antarctic Expedition (January–February 2000), *Sci. Mar.*, *66*(2), 123–133, doi:10.3989/scimar.2002.66n2123.
Schartau, M., P. Wallhead, J. Hemmings, U. Löptien, I. Kriest, S. Krishna, B. A. Ward, T. Slawig, T., and A. Oschlies (2016), Reviews and syntheses: Parameter identification in marine planktonic ecosystem modelling, *Biogeosci. Discuss.*, 1–79, doi:10.5194/bg-2016-242.
Schine, C. M. S., G. van Dijken, and K. R. Arrigo (2015), Spatial analysis of trends in primary production and relationships with large-scale climate variability in the Ross Sea, Antarctica (1997–2013), *J. Geophys. Res. Oceans*, *120*, 1–19, doi:10.1002/2015JC011014.
Sedwick, P. N., N. S. Garcia, S. F. Riseman, C. M. Marsay, and G. R. DiTullio (2007), Evidence for high iron requirements of colonial Phaeocystis antarctica at low irradiance, *Biogeochemistry*, *83*, 83–97, doi:10.1007/s10533-007-9081-7.
Sedwick, P. N., et al. (2011), Early season depletion of dissolved iron in the Ross Sea polynya: Implications for iron dynamics on the Antarctic continental shelf, *J. Geophys. Res.*, *116*, C12019, doi:10.1029/2010JC006553.
Sinclair, K. E., N. A. N. Bertler, and T. D. van Ommen (2012), Twentieth-century surface temperature trends in the western Ross Sea, Antarctica: Evidence from a high-resolution ice Core, *J. Clim.*, *25*(10), 3629–3636, doi:10.1175/JCLI-D-11-00496.1.
Sinclair, K. E., N. A. N. Bertler, M. M. Bowen, and K. R. Arrigo (2014), Twentieth century sea-ice trends in the Ross Sea from a high-resolution, coastal ice-core record, *Geophys. Res. Lett.*, *41*, 3510–3516, doi:10.1002/2014GL059821.
Smith, W. O., Jr., and R. B. Dunbar (1998), The relationship between new production and vertical flux on the Ross Sea continental shelf, *J. Mar. Syst.*, *17*, 445–457, doi:10.1016/S0924-7963(98)00057-8.
Smith, W. O., Jr., and L. I. Gordon (1997), Hyperproductivity of the Ross Sea (Antarctica) polynya during austral spring, *Geophys. Res. Lett.*, *24*(3), 233–236, doi:10.1029/96GL03926.
Smith, W. O., D. M. Nelson, and S. Mathot (1999), Phytoplankton growth rates in the Ross Sea, Antarctica, determined by independent methods: Temporal variations, *J. Plankton Res.*, *21*(8), 1519–1536, doi:10.1093/plankt/21.8.1519.
Smith, W. O., Jr., J. Marra, M. R. Hiscock, and R. T. Barber (2000), The seasonal cycle of phytoplankton biomass and primary productivity in the Ross Sea, Antarctica, *Deep Sea Res., Part II*, *47*(15–16), 3119–3140, doi:10.1016/S0967-0645(00)00061-8.
Smith, W. O., Jr., M. R. Dennett, S. Mathot, and D. A. Caron (2003a), The temporal dynamics of the flagellated and colonial stages of *Phaeocystis antarctica* in the Ross Sea, *Deep Sea Res., Part II*, *50*(3–4), 605–617, doi:10.1016/S0967-0645(02)00586-6.
Smith, W. O., Jr., M. S. Dinniman, J. M. Klinck, and E. Hofmann (2003b), Biogeochemical climatologies in the Ross Sea, Antarctica: Seasonal patterns of nutrients and biomass, *Deep Sea Res., Part II*, *50*(22–26), 3083–3101, doi:10.1016/j.dsr2.2003.07.010.
Smith, W. O., Jr., A. R. Shields, J. A. Peloquin, G. Catalano, S. Tozzi, M. S. Dinniman, and V. L. Asper (2006), Interannual variations in nutrients, net community production, and biogeochemical cycles in the Ross Sea, *Deep Sea Res., Part II*, *53*, 815–833, doi:10.1016/j.dsr2.2006.02.014.
Smith, W. O., Jr., M. S. Dinniman, S. Tozzi, G. R. DiTullio, O. Mangoni, M. Modigh, and V. Saggiomo (2010), Phytoplankton photosynthetic pigments in the Ross Sea: Patterns and relationships among functional groups, *J. Mar. Syst.*, *82*(3), 177–185, doi:10.1016/j.jmarsys.2010.04.014.
Smith, W. O., Jr., A. R. Shields, J. C. Dreyer, J. A. Peloquin, and V. Asper (2011), Interannual variability in vertical export in the Ross Sea: Magnitude, composition, and environmental correlates, *Deep Sea Res., Part I*, *58*, 147–159, doi:10.1016/j.dsr.2010.11.007.
Smith, W. O., Jr., S. Tozzi, M. C. Long, P. N. Sedwick, J. A. Peloquin, R. B. Dunbar, D. A. Hutchins, Z. Kolber, and G. R. DiTullio (2013), Spatial and temporal variations in variable fluoresence in the Ross Sea (Antarctica): Oceanographic correlates and bloom dynamics, *Deep Sea Res., Part I*, *79*, 141–155, doi:10.1016/j.dsr.2013.05.002.
Smith, W. O., Jr., M. S. Dinniman, E. E. Hofmann, and J. M. Klinck (2014a), The effects of changing winds and temperatures on the oceanography of the Ross Sea in the 21st century, *Geophys. Res. Lett.*, *41*, 1624–1631, doi:10.1002/2014GL059311.
Smith, W. O., Jr., et al. (2014b), Multiplatform, multidisciplinary investigations of the impacts of Modified Circumpolar Deep Water in the Ross Sea, Antarctica, *Oceanography*, *27*(2), 180–185, doi:10.5670/oceanog.2014.36.
Smith, W. O., Jr., D. J. McGillicuddy Jr., E. B. Olson, V. Kosnyrev, E. E. Peacock, and H. M. Sosik (2017), Mesoscale variability in intact and ghost colonies of *Phaeocystis antarctica* in the Ross Sea: Distribution and abundance, *J. Mar. Syst.*, *166*, 97–107, doi:10.1016/j.jmarsys.2016.05.007.
Spreen, G., L. Kaleschke, and G. Heygster (2008), Sea ice remote sensing using AMSR-E 89-GHz channels, *J. Geophys. Res.*, *113*, C02S03, doi:10.1029/2005JC003384.
Stammerjohn, S. E., D. G. Martinson, R. C. Smith, X. Yuan, and D. Rind (2008), Trends in Antarctic annual sea ice retreat and advance and their relation to El Niño–Southern Oscillation and Southern Annular Mode variability, *J. Geophys. Res.*, *113*, C03S90, doi:10.1029/2007JC004269.
Stevens, C. J., E. A. Pakhomov, K. V Robinson, and J. A. Hall (2015), Mesozooplankton biomass, abundance and community composition in the Ross Sea and the Pacific sector of the Southern Ocean, *Polar Biol.*, *38*(3), 275–286, doi:10.1007/s00300-014-1583-x.
Stow, C. A., J. Jolliff, D. J. McGillicuddy Jr., S. C. Doney, J. I. Allen, M. A. M. Friedrichs, K. A. Rose, and P. Wallhead (2009), Skill assessment for coupled biological/physical models of marine systems, *J. Mar. Syst.*, *76*(1–2), 4–15, doi:10.1016/j.jmarsys.2008.03.011.

Sweeney, C., D. A. Hansell, C. A. Carlson, L. A. Codispoti, L. I. Gordon, J. Marra, F. J. Millero, W. O. Smith Jr., and T. Takahashi (2000), Biogeochemical regimes, net community production and carbon export in the Ross Sea, Antarctica, *Deep Sea Res., Part II*, *47*(15–16), 3369–3394, doi:10.1016/S0967-0645(00)00072-2.

Tagliabue, A., and K. R. Arrigo (2003), Anomalously low zooplankton abundance in the Ross Sea: An alternative explanation, *Limnol. Oceanogr.*, *48*(2), 686–699, doi:10.4319/lo.2003.48.2.0686.

Tang, K. W., W. O. Smith Jr., D. T. Elliott, and A. R. Shields (2008), Colony size of *Phaeocystis antarctica* (Prymnesiophyceae) as influenced by zooplankton grazers, *J. Phycol.*, *44*(6), 1372–1378, doi:10.1111/j.1529-8817.2008.00595.x.

Winton, V. H. L., G. B. Dunbar, N. A. N. Bertler, M.-A. Millet, B. Delmonte, C. B. Atkins, J. M. Chewings, and P. Andersson (2014), The contribution of aeolian sand and dust to iron fertilization of phytoplankton blooms in southwestern Ross Sea, Antarctica, *Global Biogeochem. Cycles*, *28*, 423–436, doi:10.1002/2013GB004574.

Xiao, Y., and M. A. M. Friedrichs (2014), Using biogeochemical data assimilation to assess the relative skill of multiple ecosystem models in the Mid-Atlantic Bight: Effects of increasing the complexity of the planktonic food web, *Biogeosciences*, *11*(11), 3015–3030, doi:10.5194/bg-11-3015-2014.

Xu, K., F.-X. Fu, and D. A. Hutchins (2014), Comparative responses of two dominant Antarctic phytoplankton taxa to interactions between ocean acidification, warming, irradiance, and iron availability, *Limnol. Oceanogr.*, *59*(6), 1919–1931, doi:10.4319/lo.2014.59.6.1919.

Yool, A., E. E. Popova, and T. R. Anderson (2011), MEDUSA-1.0: A new intermediate complexity plankton ecosystem model for the global domain, *Geosci. Model Dev.*, *4*(2), 381–417, doi:10.5194/gmd-4-381-2011.

Zhu, Z., K. Xu, F.-X. Fu, J. L. Spackeen, D. A. Bronk, and D. A. Hutchins (2016), A comparative study of iron and temperature interactive effects on diatoms and *Phaeocystis antarctica* from the Ross Sea, Antarctica, *Mar. Ecol. Prog. Ser.*, *550*, 39–51, doi:10.3354/meps11732.